

Quantum rotation of HCN and DCN in ^4He

R. E. Zillich and K. B. Whaley

Department of Chemistry, University of California, Berkeley, California 94720, USA

(Received 3 September 2003; revised manuscript received 15 December 2003; published 23 March 2004)

We present calculations of rotational absorption spectra of the molecules HCN and DCN in superfluid ^4He , using a combination of the diffusion Monte Carlo method for ground-state properties and an analytic many-body method (correlated basis function theory) for the excited states. Our results agree with the experimentally determined effective moment of inertia which has been obtained from the $J=0\rightarrow 1$ spectral transition. The correlated basis function analysis shows that, unlike heavy rotors such as OCS, the $J=2$ and higher rotational excitations of HCN and DCN have high-enough energy to strongly couple to rotons, leading to large shifts of the lines and accordingly to anomalous large spectroscopic distortion constants, to the possibility of roton-maxon bands, and of secondary peaks in the absorption spectra for $J=2$ and $J=3$.

DOI: 10.1103/PhysRevB.69.104517

PACS number(s): 67.40.Yv, 05.30.Jp, 33.20.Bx, 34.30.+h

I. INTRODUCTION

In microwave helium nanodroplet isolation spectroscopy experiments, Conjunteau *et al.*¹ have measured the rotational excitation energy $J=0\rightarrow 1$ of HCN and DCN embedded in ^4He clusters. Their results show a reduction of this excitation energy by factors of 0.815 and 0.827 with respect to gas-phase HCN and DCN, respectively. Infrared spectroscopy experiments of HCN by Nauta and Miller² yield similar results from analysis of the rovibrational excitation of the C-H stretching mode, namely, a reduction of 0.795 in the $J=0\rightarrow 1$ energy. These fractional reductions are considerably smaller than those observed for heavier molecules such as SF_6 and OCS, where reductions by factors of ~ 3 are seen.³ The gas-phase rotational constants, $B=1.478\,222\text{ cm}^{-1}$ for HCN and $B=1.207\,780\text{ cm}^{-1}$ for DCN, are also much larger than the corresponding values for the heavier molecules (e.g., $B=0.2029\text{ cm}^{-1}$ and 0.0911 cm^{-1} for OCS and SF_6 , respectively). The widely observed reduction in B is understood to be due to the interaction of the molecule with the surrounding ^4He atoms.⁴ For the heavier molecules it has been found that calculations based on the microscopic two-fluid theory⁵ can reproduce the effective rotational constant B_{eff} .^{4,6} For some heavy linear rotors, a semiclassical hydrodynamical analysis that combines a classical treatment of the molecular rotation with a quantum calculation of helium solvation density approximately reproduced the moment of inertia increase measured in experiments (see Table I in Ref. 7), although no agreement is found for the octahedral SF_6 molecule.^{4,8,9} The hydrodynamic contribution to the effective moment of inertia is found to be considerably decreased when the molecular rotation is treated quantum mechanically.¹⁰

These models for heavier molecules are based on analysis of partial or complete adiabatic following of the molecular rotational motion by helium and cannot describe the dynamics of light rotors like HCN and DCN in helium for which adiabatic following does not hold.¹¹ Furthermore, infrared spectra of HCN² and acetylene, C_2H_2 ,¹² and other light molecules show a small splitting of the rovibrational $R(0)$ line which cannot be accounted for by these theoretical approaches that focus on the calculation of the helium-induced

increase of the moment of inertia. In Ref. 13, a detailed investigation of the effects of the finite ^4He environment on rotational excitations showed that both hydrodynamic coupling of translational and rotational motion and the anisotropy of the effective interaction between the molecule and the finite ^4He cluster, can result in splitting of the $R(0)$ spectral line (corresponding to the $J=0\rightarrow 1$ transition) into $M=0$ and $M=\pm 1$ contributions. However, the observed line shapes could not be explained in the case of HCN, although good agreement was found for the line shape of the $R(0)$ transition of the heavier rotor OCS.

The molecules HCN and DCN are light rotors, possessing large zero-point motion. Therefore, calculation of the ground state already requires a full quantum-mechanical treatment of the molecular rotations.¹⁴ Furthermore, for the rotational excitations, the spacing between the rotational energy levels is large, of similar magnitude as the roton energy of bulk helium [the roton gap is 8.7 K Ref. (15)]. This introduces the possibility of direct coupling between the roton states and the molecular rotational levels of light molecules. The coupling between phonons in ^4He and molecular rotational levels was analyzed perturbatively in Ref. 16, where it was shown that the lower density of phonon states in ^4He relative to that of particle-hole states in ^3He leads to a much smaller coupling of molecular rotational transitions to excitations of the quantum liquid for the Bose system. This provided a rationale for the observation of sharp rotational lines in infrared molecular spectra in the bosonic ^4He environment, but not in the fermionic ^3He environment. The specifics of the dispersion relation in ^4He were not incorporated in this perturbative analysis. In particular, only a linear phonon spectrum was employed, and the maxon and roton excitations were not taken into account. To allow for the possibility of coupling to maxons and rotons when calculating the response to the motion of these light molecules, it is evident that helium cannot simply be treated as a classical frictionless fluid possessing long-wavelength hydrodynamic modes, nor by a quantum fluid possessing quantized phonons with linear dispersion. We must therefore describe the coupled dynamics of the molecule and the strongly correlated helium quantum fluid with true quantum many-body theory, i.e., in principle, we must solve the $(N+1)$ -body Schrodinger equation.

Quantum Monte Carlo is one such fully quantum approach. Zero-temperature quantum Monte Carlo calculations for the rotational motion of a molecule doped into a finite cluster of helium have been carried out successfully for a variety of small molecules,^{11,14,17,18} in which excitation energies have been obtained with the POITSE (projection operator imaginary time spectral evolution) method¹⁹ or similar spectral evolution approaches.¹⁸ For HCN in helium clusters, rotational constants B_{eff} have been obtained for clusters consisting of up to $N=25$ ^4He atoms.¹⁴ However, in marked contrast to the heavier OCS and SF_6 molecules for which the large droplet value is arrived at well before the first solvation shell ($N\sim 20$) is complete,^{17,18,20} convergence to the experimental value of B for HCN in large ^4He clusters of several thousands of ^4He atoms was not yet found at $N=25$. This very different behavior accentuates the distinction between a light and a heavy rotor, and suggests that different physics may underlie the reduction in B for a light molecule. This, combined with the technical difficulties of making POITSE calculations for large clusters and hence to follow the small cluster B value to convergence with increasing size, motivates development of a more analytic approach that is suitable for implementation in the bulk limit. With an analytical approach, implementation is generally simpler in the bulk limit $N\rightarrow\infty$ than in a large finite system because of the higher symmetry. However, it is then necessary to recognize that derivation of an analytical model from the $(N+1)$ -body Schrödinger equation is necessarily approximative and this may affect the quantitative accuracy of our results.

The method we apply here to the rotational dynamics of HCN in helium (1 linear molecule + N spherical atoms) is a combination of the correlated basis function (CBF) theory [also called (time-dependent) hypernetted chain/Euler-Lagrange (HNC/EL) method] with diffusion Monte Carlo (DMC) ground-state calculations. The CBF method can be formulated as an energy functional approach to solving the many-body Schrödinger equation. In contrast to the formulation of density-functional theory (DFT) that is generally applied to helium systems,^{21,22} CBF theory eliminates the need for a semiempirical correlation energy functional by expressing the energy functional not only in terms of the one-body density, but also in terms of pair densities and, if necessary for quantitative agreement, also of triplet densities. Similarly to DFT, the stationary version of CBF yields the ground-state energy and structure, while the time-dependent extension of CBF yields excited states.

As an analytic approach to the many-body problem, CBF theory requires relatively little computational effort to solve the equations of motion, once these have been derived. The CBF method yields ground-state quantities such as the ground-state energy, the chemical potentials, and the pair-distribution functions. Calculation of excitations in CBF yields not only excitation energies, but also the density-density response function, and from that the dynamic structure function for pure ^4He and the absorption spectrum of the dopant molecule, as will be shown explicitly below. Although CBF theory is not an exact method, quantitative agreement has been found for a variety of quantities relevant to ^4He systems. These include ground state and collective

excitations in bulk ^4He ,^{23,24} excitations in ^4He films^{25–28} and clusters,^{29–31} and translational motion of atomic impurities in ^4He .³² This generates confidence that CBF theory may allow quantitative calculations of the rotational dynamics of dopant molecules for rotational energies in the range of the phonon-maxon-rotor regime. In the case of HCN/DCN, this means for quantum numbers up to $J=3$. Combining CBF theory for excitations with exact ground-state quantities calculated by DMC may also be expected to improve the accuracy of CBF excitations.

In this paper, we restrict ourselves to the simpler case of HCN/DCN in bulk ^4He , where translational symmetry is preserved and the analytic CBF calculations become correspondingly simpler, as opposed to HCN/DCN in ^4He clusters. This therefore precludes the calculation of inhomogeneous line broadening and possible line splitting caused by the inhomogeneous environment of the cluster.¹³

The structure of the paper is as follows. The derivation of the rotation excitation spectrum of a single linear molecule in bulk helium is presented in Sec. II. This analysis is related to the derivation of the translational excitation spectrum of an atom coupling to the phonon-rotor excitations in bulk helium, which has been discussed in detail in Ref. 32. In Secs. II A and II B, we derive the CBF equations for the excitation spectrum of a linear rotor solvated in bulk ^4He and for its absorption spectrum, respectively. In Sec. II C, we describe how the CBF theory is combined with DMC calculations of ground-state input quantities in order to obtain excitations and absorption spectra.

In Sec. III, we report the DMC results for the ground-state quantities for HCN and DCN. Section IV describes the results of the “marriage” of CBF and DMC for rotational excitations. We present and discuss the excitation energies in Sec. IV A and the absorption spectra in Sec. IV B. In a direct analogy with the definition of an effective mass of an effective free particle from the momentum dependence of the excitation energy $E(q)$, it is common to obtain an effective rotational constant B_{eff} of an effective linear rotor from analysis of one or more spectral transition energies. This was done in Ref. 1 using the experimentally observed $R(0)$ ($J=0\rightarrow 1$) spectral line. We present our corresponding results for B_{eff} obtained from the calculated $J=0\rightarrow 1$ transition energies in Sec. IV C. Our calculated values of B_{eff} are in good agreement with the experimental values, indicating that the reduction in B_{eff} relative to the gas phase B for these light molecules derives primarily from coupling to the collective modes of ^4He . This is a very different situation from that for heavier molecules, where the reduction in B_{eff} derives from coupling to some local helium density that adiabatically follows the molecular rotation,³³ a phenomenon that may be formally regarded as coupling to ^4He modes which are localized around the molecule. The present analysis thus indicates that there is indeed a different physics responsible for the reduction in rotational constants for light molecules than for heavy molecules in ^4He . A second significant feature of the CBF results is that, although we find that the energy spectrum still has the same symmetry as a linear rotor, i.e., there is no splitting of the M states within a given level in bulk ^4He , it is evident that nevertheless the J dependence of

the rotational energy $E(J)$ deviates considerably from that of an effective rigid linear rotor spectrum, $B_{\text{eff}}J(J+1)$, when a fit of B_{eff} to more than one J level is made. In particular, we find that the coupling to the roton and maxon collective excitations for higher J levels gives rise to extremely large effective ‘‘centrifugal distortion’’ terms that modify this rigid rotor form. The analysis of this deviation from the rigid rotor spectrum is discussed in detail in Sec. IV D.

Lastly, in Sec. IV F, we introduce a pseudohydrodynamic model that includes only phonon modes of ^4He but no maxon/roton modes in the CBF calculation. This provides a reference point that allows us to independently assess the effect of the maxon/roton excitations on molecule rotations. The changes in the effective rotational constants B and D relative to the gas-phase values deriving from this pseudohydrodynamic dispersion model are much reduced relative to the corresponding changes found with the true dispersion curve for ^4He , and the value of B_{eff} is no longer in such good agreement with the experimentally measured value. (D_{eff} was not experimentally accessible for HCN in the experiments to date.^{1,2}) This provides additional evidence for the critical role of the maxon/roton excitations in the reduction of B_{eff} for HCN. We summarize and provide conclusions in Sec. V.

II. THEORY

The CBF method is a microscopic quantum theory for the ground state and excitations of a many-body system. By ‘‘microscopic’’ we mean that there is no input other than the Hamiltonian, and the output quantities are expectation values with respect to the ground state or an excited state, such as energy, density, etc. In practice, approximations are necessary in order to render the CBF equations soluble. We will point out these approximations as we introduce them.

In our case the Hamiltonian for N ^4He atoms with coordinates \mathbf{r}_i , $i=1, \dots, N$ and a linear molecule at position \mathbf{r}_0 and orientation $\Omega=(\theta, \phi)$ in the laboratory frame takes the form

$$H = B\hat{L}^2 - \frac{\hbar^2}{2M}\nabla_0^2 + \sum_{i=1}^N V_X(\mathbf{r}_0 - \mathbf{r}_i, \Omega) + H_B, \quad (2.1)$$

where B is the rotational constant of the free linear rotor, \hat{L} is the angular momentum operator, M is the mass of the rotor, and V_X is the molecule- ^4He interaction potential. For HCN-He, we use the 1E8 potential of Atkins and Hutson³⁴ obtained from fitting to *ab initio* calculations of Drucker *et al.*³⁵ For DCN-He, we use the same potential [same equilibrium nuclear positions, $r_{CH}=1.064 \text{ \AA}$ and $r_{CN}=1.156 \text{ \AA}$ (Ref. 35)] and merely transform the Jacobi coordinates (r, α) to take into account the change of the center of mass. $r=|\mathbf{r}_0 - \mathbf{r}_i|$ is the helium distance from the molecule center of mass, α is the angle between the vector r and the molecular axis, measured from the hydrogen end of the molecule.

The operator H_B is the pure helium Hamiltonian,

$$H_B = -\frac{\hbar^2}{2m} \sum_{i=1}^N \nabla_i^2 + \sum_{i<j} V_{\text{He}}(|\mathbf{r}_i - \mathbf{r}_j|), \quad (2.2)$$

where m is the mass of a ^4He atom and V_{He} is the ^4He - ^4He interaction, for which we use the potential of Ref. 36.

The CBF method has been explained in detail in a number of papers,^{23,37-41} therefore we limit ourselves to giving only a very brief overview here. The starting point is to obtain the ground-state wave function of the $(N+1)$ -body system, here

$$\Psi_0 = \Psi_0(\mathbf{r}_0, \mathbf{r}_1, \dots, \mathbf{r}_N, \Omega). \quad (2.3)$$

In the framework of CBF theory, Ψ_0 is expressed in a Jastrow-Feenberg form, i.e., expressed in terms of correlations,

$$\Psi_0 = \exp \frac{1}{2} \left[\sum_{i<j} u_2(\mathbf{r}_i, \mathbf{r}_j) + \sum_{i<j<k} u_3(\mathbf{r}_i, \mathbf{r}_j, \mathbf{r}_k) + \dots + \sum_{i=1}^N u_2^X(\mathbf{r}_0, \mathbf{r}_i, \Omega) + \sum_{i<j} u_3^X(\mathbf{r}_0, \mathbf{r}_i, \mathbf{r}_j, \Omega) + \dots \right]. \quad (2.4)$$

Here the molecule is referred to as X , with center-of-mass translation coordinate \mathbf{r}_0 and angular orientation Ω defined above. The definition of the n -particle correlations u_n and u_n^X is made unique by requiring that u_n vanishes if one of its coordinates is separated from the rest. Furthermore, it provides an exact representation of the ground state when all correlations up to $n=N$ are summed, i.e., up to u_N . However, even for the strongly correlated ^4He ground state, correlations between up to just three particles are sufficient to obtain quantitative agreement of the energy and the pair-distribution function³⁸ of bulk ^4He with experiments and Monte Carlo simulations. The correlations u_n are obtained by solving the Euler-Lagrange equations, which can be written formally as

$$\frac{\delta E}{\delta u_n(\mathbf{r}_1, \dots, \mathbf{r}_n)} = 0, \quad (2.5)$$

(and similarly for δu_n^X), where E is the expectation value of the Hamiltonian, $\langle \Psi_0 | H | \Psi_0 \rangle$, and $n \leq 3$. The resulting Euler-Lagrange equations (2.5) are coupled nonlinear integro-differential equations and can be solved iteratively. Derivation of a formulation of Eqs. (2.5) that is appropriate for numerical solution can be found in Ref. 40. However, in the present ‘‘marriage’’ of CBF and DMC, solution of Eqs. (2.5) is not necessary since the ground-state properties are calculated by DMC.

A. Excited states

The primary aim of this paper is to employ CBF theory in the search for excitations of the molecule-helium system. The excitations can be obtained by generalizing the ground state form, Eq. (2.4), to time-dependent correlations, i.e., $u_2 = u_2(\mathbf{r}_1, \mathbf{r}_2; t)$, etc. By allowing a time-dependent external perturbation potential $V^{(\text{ext})}(\mathbf{r}_0, \Omega; t)$ to act on the molecule, we can then use linear response theory⁴² to obtain excitation energies involving motions of the molecule. Linear response relies on the knowledge of the ground state, which we as-

sume to have calculated according to the above recipe or by DMC (see Sec. II C) or other means and which is then weakly perturbed. The perturbed wave function can therefore be written as

$$\Psi(t) = \frac{e^{\delta U(t)/2} \Psi_0}{\langle \Psi_0 | e^{\text{Re } \delta U(t)} | \Psi_0 \rangle}, \quad (2.6)$$

where the *excitation operator* $\delta U(t)$ is given by

$$\delta U(t) = \delta u_1(\mathbf{r}_0, \Omega; t) + \sum_{i=1}^N \delta u_2(\mathbf{r}_0, \mathbf{r}_i, \Omega; t). \quad (2.7)$$

Note that we have dropped the X superscript from the two-particle molecule-helium correlation u_2 . We will continue to do this from here on, using the presence of the molecular coordinates \mathbf{r}_0 and Ω in $\delta u_1(\mathbf{r}_0, \Omega; t)$ and $\delta u_2(\mathbf{r}_0, \mathbf{r}_i, \Omega; t)$ to distinguish helium-molecule from helium-helium correlation terms. Note also that unlike the ground-state wave function Ψ_0 , the excited state $\Psi(t)$ does not possess the translational and rotational symmetry of the full Hamiltonian H . Therefore it is convenient to separate $\delta U(t)$ into a one-body term δu_1 and two-body correlations δu_2 according to Eq. (2.7). Time-dependent correlations between more than two particles can also be formally written down and added to Eq.

(2.7), but would give rise to numerically intractable equations. Consequently, we restrict ourselves to two-body correlations in $\delta U(t)$ here.

The two terms in Eq. (2.7) give rise to two Euler-Lagrange equations that are obtained by functional minimization of the action integral

$$\delta \mathcal{L} = \delta \int_{t_1}^{t_2} dt \langle \Psi(t) | H + V^{(\text{ext})}(t) - i\hbar \frac{\partial}{\partial t} | \Psi(t) \rangle = 0 \quad (2.8)$$

with respect to δu_1 and δu_2 . The action integral of a spherical impurity (^3He and atomic hydrogen) in bulk ^4He can be found in Refs. 32 and 43. We shall refer to this reference integral for a spherical impurity as \mathcal{L}_0 . For a linear molecule in helium, the situation is complicated (i) by the additional rotational kinetic energy term in the Hamiltonian,

$$H_0^{\text{rot}} = B\hat{L}^2 = -B \left[\frac{1}{\sin \theta} \frac{\partial}{\partial \theta} \left(\sin \theta \frac{\partial}{\partial \theta} \right) + \frac{1}{\sin^2 \theta} \frac{\partial^2}{\partial \phi^2} \right], \quad (2.9)$$

and (ii) by the breaking of the rotational symmetry of the ground-state distribution of ^4He atoms around the molecule. Similarly to the derivation of \mathcal{L}_0 ,³² we find for the expansion of \mathcal{L} to second order in δU :

$$\begin{aligned} \mathcal{L} = & \mathcal{L}_0 + \frac{1}{4} B \int_{t_1}^{t_2} dt \left\{ \int d0 d\Omega \rho^X \left[|\partial_\theta \delta u_1(0, \Omega)|^2 + \frac{|\partial_\phi \delta u_1(0, \Omega)|^2}{\sin^2 \theta} \right] + \int d0 d\Omega d1 \rho_2(0, 1, \Omega) \left[[\partial_\theta \delta u_1^*(0, \Omega)] \right. \right. \\ & \times [\partial_\theta \delta u_2(0, 1, \Omega)] + \text{c.c.} + \left. \left. \left(\frac{\partial_\phi \delta u_1^*(0, \Omega)}{\sin \theta} \right) \left(\frac{\partial_\phi \delta u_2(0, 1, \Omega)}{\sin \theta} \right) + \text{c.c.} + \left| \partial_\theta \delta u_2(0, 1, \Omega) \right|^2 + \frac{|\partial_\phi \delta u_2(0, 1, \Omega)|^2}{\sin^2 \theta} \right] \right. \\ & + \int d0 d\Omega d1 d2 \rho_3(0, 1, 2, \Omega) \left[[\partial_\theta \delta u_2^*(0, 1, \Omega)] [\partial_\theta \delta u_2(0, 2, \Omega)] + \text{c.c.} + \left. \left(\frac{\partial_\phi \delta u_2^*(0, 1, \Omega)}{\sin \theta} \right) \left(\frac{\partial_\phi \delta u_2(0, 2, \Omega)}{\sin \theta} \right) \right] \right\} \\ & + \int_{t_1}^{t_2} dt \int d0 d\Omega \rho_1 [\delta U](0, \Omega) V^{(\text{ext})}(0, \Omega), \end{aligned}$$

where for simplicity we abbreviated the functional arguments \mathbf{r}_i by i , and have omitted the time argument. $\rho_2(0, 1, \Omega)$ and $\rho_3(0, 1, 2, \Omega)$ are the ground-state probability densities of one and two ^4He atoms around the molecule, respectively, defined as

$$\rho_2(0, 1, \Omega) = \frac{N}{\mathcal{N}} \int d2 \dots dN |\Psi_0(0, 1, \dots, N, \Omega)|^2, \quad (2.10)$$

$$\begin{aligned} \rho_2(0, 1, 2, \Omega) \\ = \frac{N(N-1)}{\mathcal{N}} \int d3 \dots dN |\Psi_0(0, 1, \dots, N, \Omega)|^2, \end{aligned} \quad (2.11)$$

where \mathcal{N} is the normalization integral of Ψ_0 .

$$\rho_1 [\delta U](0, \Omega) = \rho^X + \text{Re} \delta \tilde{\rho}_1(0, \Omega) \quad (2.12)$$

is the time-dependent probability density of the molecule expanded to first order in δU , where we have defined the complex density fluctuation

$$\delta \tilde{\rho}_1(0, \Omega) = \rho^X \delta u_1(0, \Omega) + \int d1 \rho_2(0, 1, \Omega) \delta u_2(0, 1, \Omega), \quad (2.13)$$

and $\rho^X = 1/V$ and $\rho = N/V$ are the constant ground-state densities of the molecule and of the ^4He atoms, respectively, in the normalization volume V .

The Euler-Lagrange equations $\delta\mathcal{L}$, i.e., the one-body and two-body equations

$$\frac{\delta\mathcal{L}}{\delta u_1^*(\mathbf{r}_0, \Omega)} = 0, \quad \frac{\delta\mathcal{L}}{\delta u_2^*(\mathbf{r}_0, \mathbf{r}_1, \Omega)} = 0, \quad (2.14)$$

describe the time-dependent response of the system to the perturbation $V^{(\text{ext})}$. The *linear response* is obtained by linearizing the equations in terms of the corresponding correlation fluctuations δu_1 and δu_2 . In the following, we bring these equations into a form where the time-dependent density fluctuation $\delta\rho_1(0, \Omega)$ is a linear functional of $V^{(\text{ext})}$. From that, excitations are derived by setting $V^{(\text{ext})} = 0$.

We first eliminate $\delta u_1(0, \Omega)$ in favor of the (complex) one-body density fluctuation Eq. (2.13). Then the linearized one-body equation of motion can be written

$$B \frac{1}{\sin\theta} \begin{pmatrix} \partial_\theta \\ \partial_\phi \end{pmatrix} \cdot \mathbf{j}^r(0, \Omega) + i \delta\tilde{\rho}_1(0, \Omega) + \nabla_0 \cdot \mathbf{j}^X(0, \Omega) - 2V^{(\text{ext})}(0, \Omega) = 0, \quad (2.15)$$

where the weak $V^{(\text{ext})}$ is any perturbation acting only on the molecular degrees of freedom and \mathbf{j}^X is the translational current fluctuation. This is defined in Ref. 32 and need not concern us for rotational excitations, as we will see explicitly below. In analogy to \mathbf{j}^X , we have defined the ‘‘rotational’’ current fluctuation

$$\mathbf{j}^r(0, \Omega) = \begin{pmatrix} \sin\theta \partial_\theta \\ 1 \\ \sin\theta \partial_\phi \end{pmatrix} \delta\tilde{\rho}_1(0, \Omega) - \int d2 \delta u_2(0, 2, \Omega) \times \begin{pmatrix} \sin\theta \partial_\theta \\ 1 \\ \sin\theta \partial_\phi \end{pmatrix} \rho_2(0, 2, \Omega). \quad (2.16)$$

$\delta\tilde{\rho}_1(0, \Omega)$ is the time-dependent density fluctuation defined in Eq. (2.13), while, due to the linearization, $\rho_2(0, 2, \Omega)$ is the ground-state pair density. The second and third terms of Eq. (2.15) stem from the variation $\delta\mathcal{L}_0/\delta u_1^*(0, \Omega)$. The density fluctuation $\delta\tilde{\rho}_1$ couples via \mathbf{j}^r and \mathbf{j}^X to the two-body equation in Eq. (2.14). The two-body equation is more lengthy:

$$\begin{aligned} 0 = & \frac{B}{\sin\theta} \partial_\theta \sin\theta \rho_2(0, 1, \Omega) \partial_\theta \frac{\delta\tilde{\rho}_1(0, \Omega)}{\rho^X} + \frac{B}{\sin^2\theta} \partial_\phi \rho_2(0, 1, \Omega) \partial_\phi \frac{\delta\tilde{\rho}_1(0, \Omega)}{\rho^X} + \frac{B}{\sin\theta} \partial_\theta \sin\theta \rho_2(0, 1, \Omega) \partial_\theta \delta u_2(0, 1, \Omega) \\ & + \frac{B}{\sin^2\theta} \partial_\phi \rho_2(0, 1, \Omega) \partial_\phi \delta u_2(0, 1, \Omega) + \int d2 \frac{B}{\sin\theta} \partial_\theta \sin\theta \rho_3(0, 1, 2, \Omega) \partial_\theta \delta u_2(0, 1, \Omega) \\ & + \int d2 \frac{B}{\sin^2\theta} \partial_\phi \rho_3(0, 1, 2, \Omega) \partial_\phi \delta u_2(0, 1, \Omega) - \int d2 \frac{B}{\rho^X} \frac{1}{\sin\theta} \partial_\theta \sin\theta \rho_2(0, 1, \Omega) \partial_\theta \rho_2(0, 2, \Omega) \delta u_2(0, 1, \Omega) \\ & - \int d2 \frac{B}{\rho^X} \frac{1}{\sin^2\theta} \partial_\phi \rho_2(0, 1, \Omega) \partial_\phi \rho_2(0, 2, \Omega) \delta u_2(0, 1, \Omega) + i\hbar \delta\tilde{\rho}_2(0, 1, \Omega) + \nabla_1 \cdot \mathbf{J}_2(0, 1, \Omega) - \frac{\delta\mathcal{L}_0^{\text{trans}}}{\delta u_2^*(0, 1, \Omega)} \\ & - 2\rho_2(0, 1, \Omega) V^{(\text{ext})}(0, \Omega). \end{aligned} \quad (2.17)$$

$\delta\mathcal{L}_0^{\text{trans}}/\delta u_2^*(0, 1, \Omega)$ represents the terms related to the translational degrees of freedom of the molecule, the derivation of which again can be found in Ref. 32. The (complex) two-body density fluctuation $\delta\tilde{\rho}_2(0, 1, \Omega)$ can be expressed as a functional of $\delta\tilde{\rho}_1(0, \Omega)$ and $\delta u_2(0, 1, \Omega)$,

$$\begin{aligned} \delta\tilde{\rho}_2(0, 1, \Omega) = & \rho_2(0, 1, \Omega) \frac{\delta\tilde{\rho}_1(0, \Omega)}{\rho^X} + \rho_2(0, 1, \Omega) \delta u_2(0, 1, \Omega) \\ & + \int d2 \left(\rho_3(0, 1, 2, \Omega) \right. \\ & \left. - \frac{1}{\rho^X} \rho_2(0, 1, \Omega) \rho_2(0, 2, \Omega) \right) \delta u_2(0, 2, \Omega), \end{aligned} \quad (2.18)$$

which follows from the definition (2.10). The ^4He -current fluctuation \mathbf{J}_2 induced by the rotating molecule is defined as

$$\mathbf{J}_2(0, 1, \Omega) = \frac{\hbar}{2m} \rho_2(0, 1, \Omega) \nabla_1 \delta u_2(0, 1, \Omega). \quad (2.19)$$

Unfortunately, solution of the coupled set of equations (2.15) and (2.17) is not feasible without further approximations to the two-body equation (2.17). In a rather drastic approximation step, we therefore expand the pair distribution

$$g(0, 1, \Omega) = \frac{\rho_2(0, 1, \Omega)}{\rho^X \rho} \quad (2.20)$$

about unity. This is commonly referred to as the ‘‘uniform limit’’ approximation.³⁷ It has the advantage of leading to a

particularly simple expression for the excitation energies in terms of a self-energy correction, and has been used in many CBF calculations of excited states of ^4He and impurities in ^4He . Therefore, this uniform limit approximation is our first candidate for simplifying Eq. (2.17). We discuss the extent of the validity of this approximation in Sec. III, where we present our DMC result for g .

When applied to the equations of motions (2.15) and (2.17), the uniform limit approximation amounts to replacing the pair-distribution function $g(0,1,\Omega)$ by unity in coordinate space, but *not* in integrals, where it is retained in full form. The triplet density in the uniform limit approximation then reads

$$\rho_3(0,1,2,\Omega) - \frac{1}{\rho^X} \rho_2(0,1,\Omega) \rho_2(0,2,\Omega) \approx \rho^X \rho \rho [g(1,2) - 1], \quad (2.21)$$

where g is the pair distribution of two ^4He atoms, regardless of the position \mathbf{r}_0 and orientation Ω of the molecule.

We can furthermore eliminate $\delta\tilde{\rho}_2(0,1,\Omega)$ in favor of $\delta\tilde{\rho}_1(0,\Omega)$ and δu_2 , using Eq. (2.18), and then make use of the one-body equation (2.16), in order to arrive at

$$\begin{aligned} 0 = & B \left(\frac{\delta\tilde{\rho}_1(0,\Omega)}{\rho^X} \right) [\partial_\theta \rho_2(0,1,\Omega)] \\ & + B \frac{1}{\sin^2\theta} \left(\frac{\delta\tilde{\rho}_1(0,\Omega)}{\rho^X} \right) [\partial_\theta \rho_2(0,1,\Omega)] \\ & + \rho^X \rho \int d2S(1,2) B \hat{L}^2 \delta u_2(0,2,\Omega) \\ & + \rho^X \rho \frac{\hbar^2}{2m} \nabla_1^2 \delta u_2(0,1,\Omega) + \frac{\hbar^2}{2M} \left(\nabla_0 \frac{\delta\tilde{\rho}_1(0,\Omega)}{\rho^X} \right) \\ & \times [\nabla_0 \rho_2(0,1,\Omega)] - \rho^X \rho \frac{\hbar^2}{2M} \int d2S(1,2) \nabla_0^2 \delta u_2(0,2,\Omega) \\ & + i\hbar \rho^X \rho \int d2S(1,2) \delta \dot{u}_2(0,2,\Omega), \end{aligned} \quad (2.22)$$

where the terms involving ∇_0 stem from $\delta\mathcal{L}_0^{\text{trans}}/\delta u_2^*(0,1,\Omega)$. Note that the explicit reference to the external field $V^{(\text{ext})}(0,\Omega)$ has now been eliminated. This means that the two-body correlation fluctuations are only driven by the one-body correlation fluctuations, which in turn are the response to $V^{(\text{ext})}(0,\Omega)$. In the above equation, S is the static structure function of ^4He in coordinate space,

$$S(|\mathbf{r}_1 - \mathbf{r}_2|) = \delta(\mathbf{r}_1 - \mathbf{r}_2) + \rho(g(|\mathbf{r}_1 - \mathbf{r}_2|) - 1), \quad (2.23)$$

$$S(k) = \int d^3r e^{i\mathbf{k}\cdot\mathbf{r}} S(r). \quad (2.24)$$

Equations (2.15) and (2.22) can now be solved by expansion in plane waves and spherical harmonics. We define

$$\delta\tilde{\rho}_1(\mathbf{r}_0, \Omega) = \sum_{J,M} \int \frac{d^3q}{(2\pi)^3} e^{i\mathbf{q}\cdot\mathbf{r}} Y_{JM}(\Omega) \delta\tilde{\rho}_{JM}(q), \quad (2.25)$$

$$V^{(\text{ext})}(\mathbf{r}_0, \Omega) = \sum_{J,M} \int \frac{d^3q}{(2\pi)^3} e^{i\mathbf{q}\cdot\mathbf{r}} Y_{JM}(\Omega) V_{JM}^{(\text{ext})}(q), \quad (2.26)$$

$$\begin{aligned} \delta u_2(\mathbf{r}_0, \mathbf{r}_1, \Omega) = & \sum_{\ell,m} \int \frac{d^3k}{(2\pi)^3} \frac{d^3p}{(2\pi)^3} e^{i\mathbf{k}\cdot\mathbf{r}_0} e^{i\mathbf{p}(\mathbf{r}_0 - \mathbf{r}_1)} \\ & \times Y_{\ell m}(\Omega) \alpha_{\ell m}(\mathbf{k}, \mathbf{p}), \end{aligned} \quad (2.27)$$

$$g(\mathbf{r}_0, \mathbf{r}_1, \Omega) - 1 = g(r, \cos\alpha) - 1 = 4\pi \sum_{\ell} (2\ell + 1)$$

$$\times P_{\ell}(\cos\alpha) \int \frac{dk k^2}{(2\pi)^3} j_{\ell}(kr) g_{\ell}(k), \quad (2.28)$$

where $\mathbf{r} = \mathbf{r}_0 - \mathbf{r}_1$ and $\cos\alpha = \mathbf{r}\cdot\Omega$.

If we restrict ourselves to an external perturbation potential that couples only to the rotational degree of freedom, i.e., $V_{\ell,m}^{(\text{ext})}(q=0) \equiv V_{\ell,m}^{(\text{ext})}$, then translational motion is not directly excited. Since in CBF theory the molecule+helium system is regarded as being in its ground state before excitation, we are therefore calculating only the purely rotationally excited states, i.e., $\delta\tilde{\rho}_{\ell,m}(q=0) \equiv \delta\tilde{\rho}_{\ell,m}$.

With the above transformations and after transforming from time to frequency, the one-body and two-body response equations (2.15) and (2.22) become coupled algebraic equations. Equation (2.15) becomes

$$\begin{aligned} \hbar\omega \delta\tilde{\rho}_{JM}(\omega) + 2V_{JM}^{(\text{ext})}(\omega) \\ = & BJ(J+1) \delta\tilde{\rho}_{JM}(\omega) + 4\pi\rho^X \rho B \sum_{\substack{\ell',m' \\ \ell,m}} (-i)^{\ell'} \\ & \times \int \frac{d^3p}{(2\pi)^3} Y_{\ell',m'}^*(\Omega-p) g_{\ell'}(p) \alpha_{\ell m}(0, \mathbf{p}; \omega) \\ & \times (-1)^M \begin{pmatrix} J & \ell' & \ell \\ -M & m' & m \end{pmatrix}, \end{aligned} \quad (2.29)$$

where we note that the translational current fluctuation \mathbf{j}^X in Equation (2.15) vanishes. Eq. (2.22) becomes

$$\begin{aligned} \left(B\ell(\ell+1) + \frac{\hbar^2 p^2}{2mS(p)} + \frac{\hbar^2 p^2}{2M} - \hbar\omega \right) \alpha_{\ell m}(0, \mathbf{p}; \omega) \\ = & -4\pi B \sum_{\substack{\lambda,\mu \\ \lambda',\mu'}} (-i)^{\lambda'} (-1)^m \begin{pmatrix} \lambda & \lambda' & \ell \\ \mu & \mu' & -m \end{pmatrix} \\ & \times Y_{\lambda',\mu'}^*(\Omega_p) \frac{\delta\tilde{\rho}_{\lambda,\mu}(\omega)}{\rho^X} \frac{g_{\lambda'}(p)}{S(p)}. \end{aligned} \quad (2.30)$$

Here the static structure factor $S(p)$ is defined in Eq. (2.24). The energy expression on the left-hand side of Eq. (2.30) contains the linear rotor spectrum $B\ell(\ell+1)$ and the translational spectrum $\hbar^2 p^2/2M$ of the free molecule in addition to the the Bijl-Feynman spectrum⁴⁴ of bulk ${}^4\text{He}$,

$$\epsilon(p) = \frac{\hbar^2 p^2}{2mS(p)}.$$

The symbols in the angular brackets result from angular integration of spherical harmonics and can be expressed as follows:

$$\left\langle \begin{matrix} \ell_1 & \ell_2 & \ell_3 \\ m_1 & m_2 & m_3 \end{matrix} \right\rangle = \sqrt{\tilde{L}(\ell_1, \ell_2, \ell_3)} \left(\begin{matrix} \ell_1 & \ell_2 & \ell_3 \\ m_1 & m_2 & m_3 \end{matrix} \right),$$

$$\tilde{L}(\ell_1, \ell_2, \ell_3) = \frac{1}{4} \bar{L}(\ell_1, \ell_2, \ell_3) [\ell_1(\ell_1+1) + \ell_2(\ell_2+1) - \ell_3(\ell_3+1)],^2 \quad (2.31)$$

$$\bar{L}(\ell_1, \ell_2, \ell_3) = \frac{(2\ell_1+1)(2\ell_2+1)(2\ell_3+1)}{4\pi} \left(\begin{matrix} \ell_1 & \ell_2 & \ell_3 \\ 0 & 0 & 0 \end{matrix} \right)^2,$$

where the expressions in round brackets are Wigner's 3- j symbols.⁴⁵ After eliminating $\alpha_{\ell m}(0, \mathbf{p})$ in Eq. (2.29) by using Eq. (2.30), we use the summation rules for the Wigner 3- j symbols to further simplify Eq. (2.29). It turns out that most of the angular quantum number summations are trivial and that the $\delta\tilde{\rho}_{JM}$ coefficients do not mix. This leads to the simple formula

$$[BJ(J+1) + \Sigma_J(\omega) - \hbar\omega] \delta\tilde{\rho}_{JM}(\omega) = 2V_{JM}^{(\text{ext})}(\omega). \quad (2.32)$$

Hence we have found the linear response of the density, $\delta\tilde{\rho}_{JM}$, to a weak perturbation of symmetry (J, M) , $V_{JM}^{(\text{ext})}$. The excitation energies of the system are obtained by setting the perturbation potential to zero and solving Eq. (2.32),

$$\hbar\omega = BJ(J+1) + \Sigma_J(\omega). \quad (2.33)$$

This has to be solved self-consistently in order to obtain the excitation energy ω_J for given J (or energies, if there exist more than one solutions for given J). These solutions correspond to the energies $E_J = \hbar\omega_J$ of the coupled molecule-helium system, in the usual spectroscopic notation with total angular momentum $\hbar J$. $\Sigma_J(\omega)$ is the self-energy

$$\Sigma_J(\omega) = -B^2 \frac{(4\pi)^2 \rho}{2J+1} \sum_{\ell} \int \frac{dp}{(2\pi)^3} \frac{p^2}{S(p)} \sum_{\ell'} \tilde{L}(J, \ell', \ell) g_{\ell'}^2(p) \times \frac{1}{B\ell(\ell+1) + \epsilon(p) + \hbar^2 p^2/2M - \hbar\omega}. \quad (2.34)$$

We note that $\Sigma_J(\omega)$ does not depend on the quantum number M anymore, and that therefore we will not observe any M splitting of the $R(0)$ line of HCN in bulk ${}^4\text{He}$. This splitting has been found in spectra of HCN in ${}^4\text{He}$ droplets as reported in Ref. 2, where it has been attributed to the finite size of the droplets.¹³ Our result for the excitation energy, Eq. (2.33), indicates that all M levels are degenerate when HCN is embedded in uniform bulk ${}^4\text{He}$. Note that infrared spectra of HCN solvated in ${}^4\text{He}$ droplets in a strong electric field show clear evidence of M splitting.² The lack of M splitting in our calculation of HCN in the homogeneous environment of bulk ${}^4\text{He}$ thus indicates that the inhomogeneous environment of finite ${}^4\text{He}$ droplets may indeed be responsible for the observed spectral splitting.

In general, the self-energy will be complex. Strictly speaking, Eq. (2.33) cannot be solved self-consistently in that case, and we can only speak in terms of the response of the system to the perturbation (i.e., laser field). The imaginary part of $\Sigma_J(\omega)$, which is the homogeneous linewidth, i.e., the inverse lifetime of the state J , results from the contour integration $\int dp$ in Eq. (2.34) when the energy denominator has a zero. At such quantum numbers p and ℓ , energy conservation allows for a decay of state J having energy $\hbar\omega_J$ into a lower rotational excitation with energy $B\ell(\ell+1)$, while exciting a phonon of energy $\epsilon(p)$ and translational motion of the molecule of energy $\hbar^2 p^2/2M$ (momentum conservation) such that $\hbar\omega_J = B\ell(\ell+1) + \epsilon(p) + \hbar^2 p^2/2M$. For all other combinations of p and ℓ , a decay would not conserve energy, thus these decay channels are closed.

The quantity \tilde{L} , Eq. (2.31), contains a Wigner 3- j symbol as well as a rotational kinetic-energy factor [the expression in the rectangular brackets on the right-hand side of Eq. (2.31)]. Combined, they obviously lead to the selection rules

$$\begin{aligned} \tilde{L}(\ell_1, \ell_2, \ell_3) &= 0, & \text{if } \ell_1 + \ell_2 + \ell_3 \text{ odd,} \\ \tilde{L}(\ell_1, \ell_2, \ell_3) &= 0, & \text{if } \ell_1, \ell_2, \ell_3 \text{ do not satisfy the triangular} \\ & & \text{condition (Ref. 45),} \end{aligned} \quad (2.35)$$

$$\tilde{L}(\ell_1, \ell_2, \ell_3) = 0, \text{ if } \ell_1 = 0 \text{ or } \ell_2 = 0.$$

It follows that $\Sigma_J(\omega) = 0$ for $J=0$, i.e., the self-energy does not renormalize the ground-state energy. The coupling of the spectra in the energy denominator is mediated by the anisotropic pair probability distribution $g(r, \cos\alpha)$, decomposed into its Legendre expansion coefficients. Furthermore, the spherical expansion coefficient $g_{\ell'=0}$ does not contribute to $\Sigma_J(\omega)$.

We note that in the self-energy part of the spectrum (2.33), $\hbar\omega_J$ couples to free rotor states, to the free translational states, and to the Bijl-Feynman spectrum of helium. Although we should not overinterpret the meaning of the individual terms in $\Sigma_J(\omega)$, in an exact expression for the correction to the rotational energy in the helium environment we would expect to find a coupling to renormalized molecular rotations and translations. We would also expect to see coupling to the exact energy spectrum of ${}^4\text{He}$, instead of

coupling to the Bijl-Feynman spectrum. Going beyond the uniform limit approximation for the probability densities might improve the molecular rotation spectrum in these respects, as has been found for other excitations in helium. These include calculations of the bulk helium spectrum²⁴ and of the effective mass of ³He impurities in ⁴He.⁴⁶ Alternatively (and much easier), we can choose a phenomenological approach and try to improve the self-energy of Eq. (2.33) by using any one or a combination of the following replacements in the energy denominator of the self-energy.

(1) In the following, we will always use the experimentally measured excitation spectrum instead of the Bijl-Feynman spectrum.

(2) We can use the dispersion of translational motion of HCN and DCN in bulk ⁴He, $\hbar^2 p^2/2M_{\text{eff}}$ instead of the free dispersion. Since we do not know of any experimental value for M_{eff} of HCN and DCN (which would be a tensor quantity), we use the bare mass M .

(3) We can use $\hbar\omega_\ell$ self-consistently instead of $B\ell(\ell+1)$. In this case, we solve $\hbar\omega = B\ell(\ell+1) + \Sigma_\ell(\omega)$ for $\hbar\omega$ at angular quantum number ℓ , and the solution $\hbar\omega_\ell$ replaces $B\ell(\ell+1)$ in the energy denominator of $\Sigma_j(\omega)$ for the next iteration; the procedure is iterated until convergence is reached for all $\hbar\omega_j$. In the case of the calculation of the effective mass of impurities in ⁴He, this phenomenological approach was shown to improve agreement with experimental results.³² However, we will see that in case for molecule rotations in ⁴He, for given J we can have several solutions ω_j of Eq. (2.33), see Appendix A. We minimize the ambivalence associated with this procedure and will not use this phenomenological improvement of the self-energy.

We discuss the dependence of the results on these phenomenological improvements in Appendix C, where B_{eff}/B_0 is calculated for various combinations of replacements 1, 2, and 3. For the rest of the paper, we apply only replacement 1.

A related concern is the missing of decay channels where localized ⁴He excitations are generated instead of a bulk helium excitation $\epsilon(p)$. Localized layer phonons and rotons have been calculated⁴⁷ and observed⁴⁸ for helium adsorbed to graphite sheets, and localized vibrations calculated for helium adsorption on aromatic molecules.⁴⁹ Since the rotation of a molecule in ⁴He involves a correlated motion of the molecule and the surrounding ⁴He atoms, it can be regarded as involving a localized “layer” excitation of the ⁴He when observed from the molecule frame. One significant difference from layer excitations of helium adsorbed to an extended substrate is that here the molecule “substrate” is so light that its motion must be taken into account (the rotational motion has been seen to have an influence on the vibrational energies for ⁴He adsorbed on the benzene molecule⁴⁹). However, decay into channels other than bulk helium excitations, such as the localized molecule-helium excitations themselves, is beyond the ansatz of Eq. (2.7) and the uniform limit approximation, as we have pointed out above. Deriving and solving the CBF equations in the frame of the molecule would allow coupling to localized excitations, although it would considerably complicate the CBF equations. An extension in this direction might allow analysis of the rotational dynamics of heavier molecules such as

OCS and extraction of the moment of inertia renormalization deriving from coupling to some adiabatically following helium.⁴ However for the light HCN molecule, our results below show good agreement with the experimental rotational constant in helium, indicating that such coupling to localized excitations is not important in this case.

B. Linear response and absorption spectrum

Once we have derived the excitation energy of molecular rotations in ⁴He from a linear response approach, we can also obtain the dynamic response function $\chi(\omega)$, which is the linear operator relating a weak perturbation $V^{(\text{ext})}$ of frequency ω and the response of the probability density $\delta\rho_1$:

$$\delta\rho_1(\omega) = \chi(\omega)V^{(\text{ext})}(\omega).$$

$\chi(\omega) = \chi'(\omega) + i\chi''(\omega)$ consists of a real part $\chi'(\omega)$ describing dispersion, and an imaginary part $\chi''(\omega) \equiv -S(\omega)$ describing absorption^{42,50} [note that our definition of $S(\omega)$ differs by a factor of π from the definition of Ref. 42]. However, we cannot simply identify the inverse of the expression in the bracket in Eq. (2.32) with $\chi(\omega)$, because $\delta\tilde{\rho}(\omega)$ is the Fourier transform of the complex density fluctuation $\delta\tilde{\rho}_1(0, \Omega)$. The *physical* density response in linear order is given by the *real part* of $\delta\tilde{\rho}_1(0, \Omega)$:

$$\delta\rho_1(0, \Omega; t) \equiv \langle \Phi(t) | \hat{\rho}_1(0, \Omega) | \Phi(t) \rangle = \text{Re} \delta\tilde{\rho}_1(0, \Omega; t).$$

Here $\hat{\rho}_1(\mathbf{r}_0, \Omega)$ is the molecule density operator, which is given in coordinate space by $\delta(\mathbf{r}_0 - \mathbf{r}'_0)\delta(\Omega - \Omega')$. The expectation value of $\hat{\rho}_1(0, \Omega)$ is the probability to find a molecule at position \mathbf{r}_0 and orientation Ω .

To obtain $\chi(\omega)$ from Eq. (2.32), we first note that

$$\delta\rho_{JM}(\omega) = \frac{1}{2} [\delta\tilde{\rho}_{JM}(\omega) + (-1)^M \delta\tilde{\rho}_{J, -M}^*(-\omega)],$$

$$[V_{J, -M}^{(\text{ext})}(-\omega)]^* = (-1)^M V_{JM}^{(\text{ext})}(\omega),$$

where we used the fact that $V^{(\text{ext})}(\Omega; t)$ is real. With relation (2.32) we find

$$\delta\rho_{JM}(\omega) = [G_J(\omega) + G_J^*(-\omega)]V_{JM}^{(\text{ext})}(\omega),$$

where $G_J(\omega)$ is the resolvent

$$G_J(\omega) = [BJ(J+1) + \Sigma_J(\omega) - \hbar\omega]^{-1}. \quad (2.36)$$

Since $G_J(\omega)$ is real for $\omega < 0$, we obtain for the dynamic response function

$$\chi_J(\omega) = G_J(\omega) + G_J(-\omega). \quad (2.37)$$

From this the absorption spectrum of a rigid linear rotor exposed to dipole ($J=1$), quadrupole ($J=2$), etc., radiation of frequency ω can be obtained as

$$S_J(\omega) = -\text{Im}\chi_J(\omega) = -\text{Im}G_J(\omega). \quad (2.38)$$

C. Marriage of DMC and CBF

Formulations of the ground-state Euler-Lagrange equations (2.5) which are suitable for numerical solution have to take advantage of the symmetries of the system under consideration. In our case this means translational symmetry and rotational symmetry around the axis of the linear molecule. Unlike the corresponding CBF calculation of excitation (2.14), the ground-state equations (2.5) cannot be linearized, due to the strongly repulsive interactions. Consequently both their formulation for a specific symmetry and their numerical solution are more demanding than the calculation of excitations. Nevertheless, the calculation of the self-energy $\Sigma_J(\omega)$ (2.34) does require knowledge of some ground-state quantities, in particular, of the ^4He - ^4He and the ^4He -molecule pair-distribution functions, $g(1,2)$ [Eq. (2.23)] and $g(0,1,\Omega)$ [Eq. (2.20)].

The ^4He - ^4He pair-distribution function $g(1,2)$ is the Fourier transform of the static structure factor $S(k)$. For bulk ^4He this has been obtained with great accuracy from neutron-scattering experiments.^{51,52} $S(k)$ has also been calculated using HCN/EL theory³² and DMC (Ref. 53) We have used the $S(k)$ at $T=0$ K from Ref. 32 as well as the experimentally determined $S(k)$ at $T=1$ K from Ref. 51. These give essentially identical results for the rotational excitation energies, i.e., the results are independent of the finer details of $S(k)$. We note that doping N ^4He atoms with a single molecule will cause only a change of $S(k)$ on the order of $O(1/N)$. Therefore we can safely use the $S(k)$ of pure ^4He in the expression for the self-energy (2.34).

We additionally need to calculate the ^4He -molecule pair-distribution function $g(0,1,\Omega)$. Here DMC is of use: DMC is easy to implement for the calculation of ground-state properties, and since it does not require prior specification of symmetries, one DMC implementation can be applied to any molecule- ^4He system with only little modification. Hence we shall employ DMC for calculation of the ground-states instead of solving equations (2.5). This effectively avoids the difficulties of solving the nonlinear Euler-Lagrange equations in a ground state calculation. We therefore use CBF theory only for excited states. The combined procedure can be summarized as follows.

Step 1. DMC for calculation of the ^4He -molecule pair distribution $g(0,1,\Omega)$.

Step 2. CBF for calculation of rotational excitations $\hbar\omega_J$ and the corresponding absorption spectrum, using as input the ^4He -molecule pair distribution $g(0,1,\Omega)$ obtained in step 1 and the ^4He - ^4He pair distribution taken from experimental neutron scattering data.^{15,54}

The energies $\hbar\omega_J$ reported for HCN and DCN in this work (Sec. IV A) are obtained using these two steps.

In addition to the approximate calculation of excitation energies and lifetimes, CBF provides us with calculation of the excitation operator δU for which $\delta U|\Phi_0\rangle$ is a good approximation of the excited-state wave function. This raises a potentially useful option for further improvement of energy calculations in these systems by direct means. We note that the representation of an excited state in terms of an excitation

operator that is made in CBF is conceptually similar to the representation made in the POITSE approach.¹⁹ In POITSE, the excitation operator provides input for a zero-temperature imaginary time correlation function calculation from which the corresponding excitation energy is obtained by inverse Laplace transformation. In CBF, the excitation operator is one of the outputs of the calculation, and it is normally discarded. Finding the appropriate excitation operator for a POITSE calculation can be a hard problem in some systems. Therefore, knowledge of a good excitation operator deriving from a high-quality CBF calculation may help considerably in reducing the computational expense as well as in simplifying the inverse Laplace transformation of a POITSE calculation. By using Eqs. (2.13), (2.27), and (2.30) one can show that within CBF the one-body term of δU in Eq. (2.7) is proportional to

$$\delta u_1(\Omega) \sim Y_{JM}(\Omega), \quad (2.39)$$

i.e., the free rotor wave function, corresponding to an excitation energy $BJ(J+1)$. Thus, it is the two-body terms of δU which are responsible for the reduction in value of the effective rotational constant B_{eff} below the free rotor value B . To date, POITSE and related calculations for rotational excitations of molecules in helium clusters^{14,17,18,55} have used only one-body excitation operators of the above form. We therefore propose that in future implementations of spectral evolution methods such as POITSE, one employs the CBF excitation operator δU of Eq. (2.7). In this situation, the output of CBF, δU , may then be used as the input to a third calculation step.

Step 3. CBF provides the excitation operator for a POITSE calculation of the exact excitation energies $\hbar\omega_J$.

We expect that because of the incorporation of molecule-helium correlations into the excitation operator within an exact calculation methodology, this should provide an improvement over the present calculations that terminate after step 2.

III. RESULTS: GROUND STATE

The implementation of DMC for a single linear molecule surrounded by ^4He follows Refs. 56 and 57 treating the molecule as a rigid body with both rotational and translational degrees of freedom. The difference is that here the system is confined to a simulation box of appropriate size and periodic boundary conditions are applied. The simulation box moves with the molecule such that the latter is kept in the center of the box (but the box does not rotate with the molecule). The size s of the simulation box can be either adjusted such that (i) the system consisting of 256 ^4He atoms and a single HCN or DCN molecule is in equilibrium, i.e., the ground-state energy is minimized with respect to variations of the box size; or such that (ii) the ^4He density reaches the asymptotic equilibrium value $\rho=0.022 \text{ \AA}^{-3}$ furthest away from the molecule (the edge of the simulation box). In the first method, the calculated quantity (the total energy) changes quadratically with the change of s , and in the second method the calculated quantity (the asymptotic density) changes linearly. The first method is thus more susceptible to errors by

construction. Furthermore, there is an uncertainty in the total energy that is largely due to the cutoff of the ${}^4\text{He}$ - ${}^4\text{He}$ interaction potential at large distances (see below). For these reasons, we chose to adjust s by the second method. In order to avoid excessive amount of calculations to find the equilibrium density (zero pressure), we choose only three box sizes, $s=22.5$ Å, 23.0 Å, and 23.5 Å. We found that the $s=23.0$ Å simulation yields edge densities closest to the equilibrium bulk value. Using one of the other box sizes did not change our results for the rotational excitation energies within the statistical error. We have used a time step of $dt=0.15$ mK for the imaginary-time evolution to the ground state. We have doubled dt and again have obtained the same result for the rotational excitation energies, thereby verifying that the DMC energies are free of finite time step bias.

Ground-state expectation values [i.e., $g(r, \cos \alpha)$] have been calculated with pure estimators using descendant weighting of importance sampled DMC according to the approach of Ref. 58. The trial wave function used here for the importance sampled DMC has the form

$$\Psi_T = \exp \frac{1}{2} \left[\sum_{i=1}^N u_1^{(T)}(|\mathbf{r}_i - \mathbf{r}_0|, \cos \alpha_i) + \sum_{i < j} u_2^{(T)}(|\mathbf{r}_i - \mathbf{r}_j|) \right], \quad (3.1)$$

with the molecule- ${}^4\text{He}$ correlation $u_1^{(T)}$ (Ref. 14) and the ${}^4\text{He}$ - ${}^4\text{He}$ correlation $u_2^{(T)}$ (Ref. 53) given by

$$u_1^{(T)}(r, \cos \alpha) = -(c/r)^5, \quad (3.2)$$

$$u_2^{(T)}(r) = -(b/r)^5 \quad (3.3)$$

with $c=7.392$ Å and $b=2.670$ Å. The precise form of the trial function is not important because we use descendant weighting for obtaining unbiased values for $g(r, \cos \alpha)$. Such an isotropic trial function was found to be adequate for previous importance sampled DMC calculations for HCN in small clusters.¹⁴ This is expected from the weak anisotropy of the HCN-He interaction. Figure 1 shows contours of the molecule-helium interaction potential V_X for HCN- ${}^4\text{He}$. For computational efficiency we introduce a cutoff for both the ${}^4\text{He}$ - ${}^4\text{He}$ interaction and its correlation $u_2^{(T)}$ at a radius $r_c=8$ Å, and replace $u_2^{(T)}$ by a smooth function⁵⁹

$$\bar{u}_2^{(T)}(r) = u_2^{(T)}(r) - u_2^{(T)}(r_c) - (r - r_c) \frac{du_2^{(T)}(r)}{dr} \Big|_{r=r_c}. \quad (3.4)$$

For completeness, we report the ground-state energetics of HCN in bulk ${}^4\text{He}$ obtained within these calculations. In order to correct the total potential energy for the error introduced by the cutoff, we assume a homogeneous ${}^4\text{He}$ equilibrium density ρ at zero pressure, and approximate the missing contribution to the total ground-state energy, $E_{\text{corr}} = (\rho/2) \int_{r_c}^{\infty} d^3r V_{\text{He}}(r)$. This is not a highly accurate correction, but the exact value of the ground state energy is immaterial for our calculation of $g(r, \cos \alpha)$. For the equilibrium

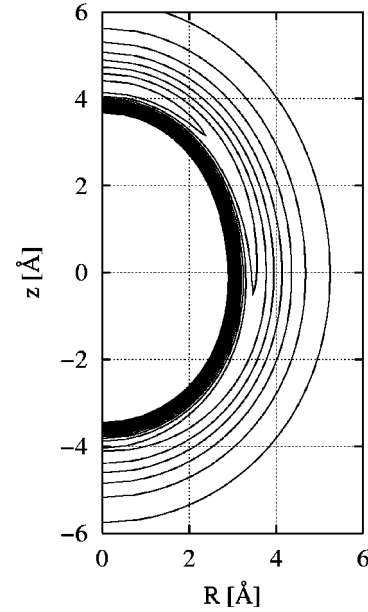


FIG. 1. Contour plot of the HCN- ${}^4\text{He}$ potential surface $V_X(R, z)$ from Ref. 34. Contour levels are shown at energy spacings of 5 K, with the outermost contour at -5 K, the next one at -10 K, etc. The linear HCN molecule is oriented along the z axis such that the hydrogen points in the positive z direction. R is the cylindrical polar radius. At $z=4.25$ Å and $R=0$ Å, the potential attains its minimum value of -42.4 K.

density $\rho=0.022$ Å⁻³, the DMC sampling yields an uncorrected ground-state energy of $E'/N = -7.35 \pm 0.006$ K. The correction is $E_{\text{corr}}/N = -0.95$ K per ${}^4\text{He}$ atom. Thus we find a total energy of approximately $E/N = -8.3$ K for both HCN and DCN. The chemical potential of the molecule μ is the difference between the energy E of molecule and helium and the energy of pure helium, $E_0 = N \times 7.2$ K at equilibrium. Hence we find $\mu \approx -282$ K for HCN and DCN in bulk ${}^4\text{He}$.

In Fig. 2, the pair distribution $g(r, \cos \alpha)$ [Eq. (2.28)] is shown for HCN in bulk ${}^4\text{He}$, simulated by 256 ${}^4\text{He}$ atoms in a box of 23.0 Å length on each side with periodic boundary conditions applied. For DCN, we used the same box size. The coordinates r and α are the radial and polar spherical coordinates in the center-of-mass frame of the HCN molecule, with the molecular symmetry axis as the z axis.

Due to the small anisotropy of the ${}^4\text{He}$ -HCN and ${}^4\text{He}$ -DCN potential, and the large zero-point rotational motion of the molecule, the pair distribution $g(r, \cos \alpha)$ is only slightly anisotropic. In Fig. 3, we show the Legendre expansion coefficients $g_\ell(r)$ of $g(r, \cos \alpha)$, whose Bessel transform is the quantity entering the calculation of the self-energy (2.34). In the limit of $B \rightarrow \infty$, the zero-point motion would completely delocalize the molecule orientation with respect to the surrounding ${}^4\text{He}$. In this situation, $g(r, \cos \alpha)$ would be isotropic, $g_{\ell > 0}(r) = 0$, and therefore the self-energy correction to B_{eff} would vanish, $B_{\text{eff}} = B$. With the large but finite B value of HCN, the Legendre expansion coefficients $g_{\ell > 0}(r)$ are not negligible. As can be seen from

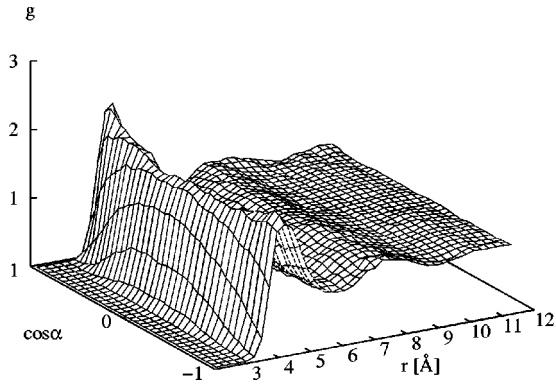


FIG. 2. Pair distribution $g(r, \cos \alpha)$ [Eq. (2.28)], between HCN and $^4\text{He}_N$, for $N=256$. r is the distance between HCN and a ^4He atom, and α is the angle between the directional vector from HCN to ^4He and the HCN axis. The HCN- ^4He interaction potential [see Fig. 1] is defined such that hydrogen is located on the positive side of molecule axis, i.e., at $\alpha=0$.

Fig. 3, the quadrupole coefficient $g_2(r)$ is the main contribution to the anisotropy of $g(r, \cos \alpha)$ for HCN.

We recall that for the derivation of the rotational self-energy expression (2.34), the uniform limit approximation was applied (see discussion in Sec. II A). For the Legendre expansion, this translates into the coordinate space approximations $g_{\ell=0}(r) \approx 1$ and $g_{\ell>0} \ll 1$. While all higher expansion coefficients $g_{\ell>0}(r)$ never exceed values of 0.2 in absolute value, $g_0(r)$ deviates from unity considerably, varying between 0 and values of almost 2. However, since, due to the selection rules, $\Sigma_J(\omega)$ is independent of $g_{\ell=0}$, we see that the extent of angular modulations in the helium solvation density are consistent with the uniform limit and that this is therefore a good approximation for the purpose of calculating purely rotational excitations of a light rotor like HCN and DCN. We note that for the heavier linear rotor OCS, which has a stronger and more anisotropic interaction with helium,⁶⁰ the angular modulation in the first layer of helium

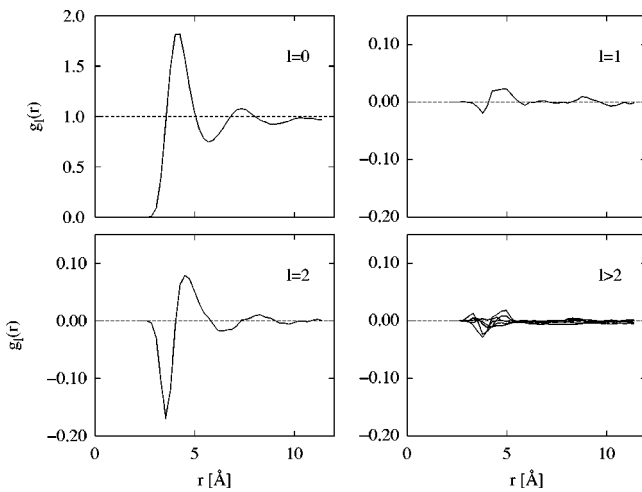


FIG. 3. Legendre expansion coefficients $g_\ell(r)$ of the pair-distribution function $g(r, \cos \alpha)$, between HCN and $^4\text{He}_N$, for $N=256$ in a cubic simulation box of length 23.0 \AA .

TABLE I. Energies of the primary rotational excitation of HCN and DCN. CBF denotes the present calculations employing CBF theory for excitations combined with exact ground-state quantities calculated by DMC, and expt. refers to the experimental values of Ref. 1.

J	HCN(CBF) (cm^{-1})	HCN(expt.) (cm^{-1})	DCN(CBF) (cm^{-1})	DCN(expt.) (cm^{-1})
1	2.53	2.407	2.08	1.998
2	6.64		5.76	
3	10.8		9.77	

around OCS is considerably larger than⁴ for HCN (Fig. 3). Hence the expansion coefficients $g_\ell(r)$ will be considerably larger and use of the uniform limit approximation would be more questionable for OCS.

IV. RESULTS: EXCITED STATES

A. Rotational energies of HCN and DCN in ^4He

The excitation energies are obtained as the solutions ω_J of Eq. (2.33). Unlike for a linear molecule in the gas phase [where $\Sigma_J(\omega)=0$], it is possible that more than one solution exists for a given J . In the following section, we will show that this is actually the case for $J=2$ and $J=3$ (and presumably for higher J 's). The existence of several solutions is not surprising considering that ω_J are the approximate excitation energies of a *many*-body system.

Table I lists the energies of the primary rotational excitation for $J=1,2,3$. By ‘‘primary’’ we refer to the excitation of lowest energy, when we find more than one solutions of Eq. (2.33). The occurrence of several lines for a given J is discussed in the following section and in Appendix A. Also shown in Table I are the respective experimental excitation energies for HCN and DCN obtained by microwave spectroscopy.¹ Only the energy for $J=1$ could be measured experimentally, because the helium cluster temperature of $T=0.38 \text{ K}$ is too low to allow appreciable population of rotationally excited states for this system.

B. Absorption spectra of HCN in ^4He

As discussed in more detail in Sec. IV E, the self-energy $\Sigma_J(\omega)$ is complex, and the excitations obtained from Eq. (2.33) are therefore not true eigenstates but decay as a result of the coupling to ^4He excitation modes. This effect is observed in the molecule absorption spectrum $S_J(\omega)$, Eq. (2.38), in the weak perturbation field $V^{(\text{ext})}$ of frequency ω .

In a spectroscopic experiment, the frequency ω of a microwave laser field is scanned to obtain the rotational spectrum. Since the wavelength is much longer than the size of the molecule, only the dipole component of $V^{(\text{ext})}(\Omega)$, corresponding to the $J=1$ component, is non-negligible. As a zero-temperature method, DMC/CBF only describes excitations from the ground state to an excited state. Hence, with the dipole field $V_{1M}^{(\text{ext})}$ acting on the molecule, we obtain only the $J=0 \rightarrow 1$ rotational excitation(s). This corresponds to the $R(0)$ spectral line. Neither the $J=1 \rightarrow 2$, $2 \rightarrow 3, \dots$ excita-

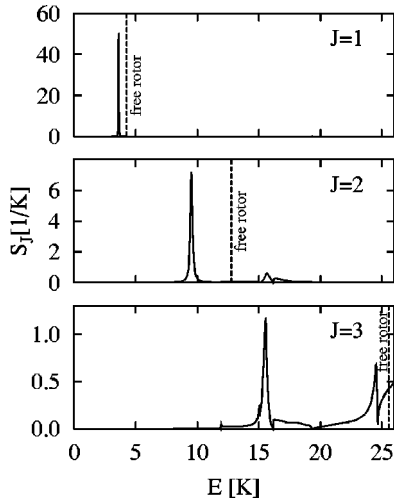


FIG. 4. The absorption spectra $S_J(\omega)$, $J=1,2,3$, for HCN in bulk ${}^4\text{He}$, where this is represented by $N=256$ ${}^4\text{He}$ in a box subject to periodic boundary conditions (see text). The dashed lines indicate the corresponding rotational excitation energies of HCN in the gas phase (Ref. 65). The spectra have been broadened by a Lorentzian, by adding a small constant imaginary part of 10 mK to the self-energy $\Sigma_J(\omega)$.

tions corresponding to $R(0), R(1), \dots$ spectral lines, nor the deexcitations $J=1 \rightarrow 0, 2 \rightarrow 1, \dots$ corresponding to the $P(1), P(2), \dots$ spectral lines are obtained directly. However, one can go from the ground state to $J=2, 3, \dots$ simply by directly applying perturbations $V_{JM}^{(\text{ext})}$, $J=2, 3, \dots$, i.e., via quadrupole-, octopole-, etc., transitions. Unlike in experiment, it is much easier in our CBF calculation to apply these multipole perturbations rather than formulate and solve the problem in a finite temperature theory. It has the added benefit that the zero-temperature absorption spectra $S_J(\omega)$ resulting from application of dipole, quadrupole, etc., perturbations are simpler to interpret than finite temperature spectra, while still containing all the information about the energetics of the system. In Fig. 4, we plot the resulting absorption spectra $S_J(\omega)$, $J=1, 2, 3$, for HCN, where we have set both the field strength $V_{JM}^{(\text{ext})}$ and the dipole moment of HCN to unity (these factors will only scale the intensities of the spectra). The DCN spectra look very similar. As we have pointed out above (Sec. II A), we correct the energy denominator of the self-energy in Eq. (2.37) by using the experimental phonon-roton spectrum instead of the Bijl-Feynman spectrum. However, we have not further replaced $B\ell(\ell+1)$ by $\hbar\omega_\ell = B\ell(\ell+1) + \Sigma_\ell(\omega_\ell)$. A detailed discussion about the effect of these and other phenomenological corrections can be found in Appendix C.

Without ${}^4\text{He}$ surrounding the molecule, we have $\Sigma_J(\omega) = 0$, i.e., the spectrum is a δ function centered at the free rotor energy,

$$\begin{aligned} S_J^{(\text{free})}(\omega) &= -\text{Im}[\hbar\omega - BJ(J+1) + i\varepsilon]^{-1} \\ &= \pi\delta(\hbar\omega - BJ(J+1)). \end{aligned} \quad (4.1)$$

In Fig. 4, the free rotor lines are indicated by dashed vertical lines.

In the CBF approximation, the self-energy $\Sigma_J(\omega)$ is non-zero with both a real and an imaginary part. The associated absorption spectrum $S_J(\omega)$ shows two kinds of features—sharp peaks and broader bands. We first analyze the sharp peaks. The origin of sharp peaks in $S_J(\omega)$ is discussed in detail in Appendix A. We show there how an imaginary part that is small relative to $BJ(J+1) + \text{Re}\Sigma_J$ leads to a Lorentzian peaked at the energy $\hbar\omega_J$, which is obtained as the solution (or one of the solutions) of $\hbar\omega - BJ(J+1) - \text{Re}\Sigma_J(\omega) = 0$. The energy $\hbar\omega_J$ can be associated with a rotational excitation of finite lifetime, which decays into a combination of a molecular $\ell < J$ state and an excitation of the helium environment. The width of the Lorentzian is given by $\text{Im}\Sigma_J(\omega_J)$ (see Sec. IV E).

In Fig. 4, the spectra $S_J(\omega)$ show sharp peaks of increasing width and decreasing height with increasing J . This indicates that the coupling of the HCN rotation to the phonon-roton spectrum of bulk ${}^4\text{He}$ is stronger for higher energies. The lowest molecular mode $J=1$ has the weakest coupling, evidenced by the fact that $S_1(\omega)$ is very close to the spectrum of a free rotor at $T=0$, i.e., it has a single sharp line. In the following section we will obtain the effective rotational constant B_{eff} from this line and compare with the corresponding experimental measurement. The exact width of the $J=1$ spectral line is subject to computational uncertainties related to the DMC ground-state calculation, as explained in Sec. IV E and therefore cannot be directly compared with the experimental line width. In contrast to the single peak seen for $J=1$, the spectra for $J=2$ and $J=3$ show several distinct sharp peaks. As explained in Appendix A, calculation of the position of a peak can result in several solutions. In some cases,²⁶ the associated peaks have very small weight, but for $J=2$ and $J=3$, we find two clearly discernible peaks. Detailed analysis of the origin of these two peaks is also presented in Appendix A. The analysis shows that this two-peak structure of $S_J(\omega)$ is a direct consequence of the divergent density of states of ${}^4\text{He}$ at the roton minimum and the maxon maximum. Coupling to these divergences effectively splits the single free peak into two, and shifts one of the resulting peaks below the roton minimum and the other above the maxon maximum. Both peaks lie very close in energy to the divergent density of states of the phonon-roton dispersion. Therefore the motion of the molecule can couple to many excitations and the molecule rotates in a dense cloud of *virtual* roton and maxon excitations. Because of energy conservation, excitation of *real* rotors and maxons is not allowed at the energies of the two peaks. If it were allowed, it would lead to immediate damping of the rotation and we would not see well-defined peaks.

We consider now the origin of the broader bands of $S_J(\omega)$ in Fig. 4. These broader bands are seen as additional features in the spectra for $J=2$ and $J=3$, between the two peaks. This is more clearly seen in Fig. 5, where the absorption spectra are now plotted all on the same scale and are shown together with the density of states for the bulk+freely translating particle excitation spectrum $\varepsilon(p) + \hbar^2 p^2/2M$ (bottom panel). In the energy range $E=12.0\text{--}15.1$ K, S_2 has a high-energy wing that is clearly aligned with the energy corresponding to maxon-roton excitations in ${}^4\text{He}$ plus a recoiling

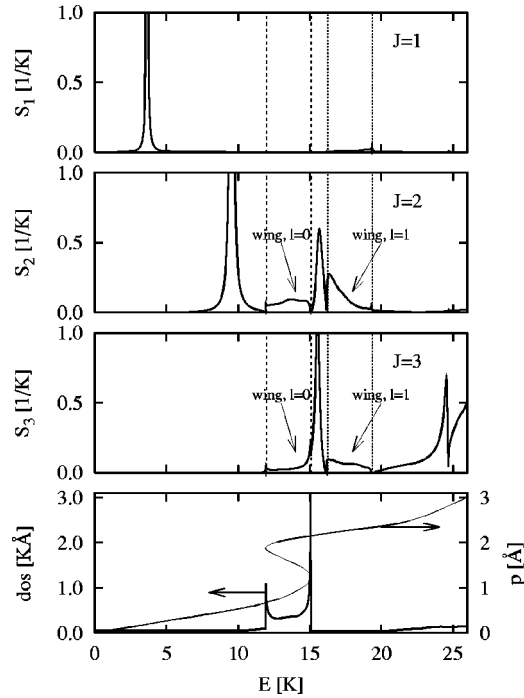


FIG. 5. The spectra $S_J(\omega)$, $J=1,2,3$, for HCN in bulk ^4He with all $S_J(\omega)$ now shown on the same scale. For details of the representation of bulk ^4He see Fig. 4 and text. The bottom panel shows in addition the dispersion curve $\varepsilon(p) + \hbar^2 p^2 / 2M$ and its density of states (“dos”) $[d\varepsilon(p)/dp + \hbar^2 p / M]^{-1}$. The vertical dashed and dotted lines indicate the onset of the roton-maxon band coupling with the $\ell=0$ (dashed lines) and the $\ell=1$ (dotted lines) rotational states of the molecule, respectively (see text).

HCN molecule. This wing structure is thus a signature of efficient coupling of the molecule to high-energy excitations in ^4He that lie between the roton minimum and the maxon maximum. Excitations of the molecule in this wing feature are virtual, i.e., the molecule remains in its ground state $\ell=0$. Another roton-maxon wing results from the coupling of the rotors and maxons with the $\ell=1$ state of the molecule. Hence this wing is shifted by $B\ell(\ell+1)=2B$ and corresponds to the generation of a high-energy ^4He excitation together with translational recoil of the molecule, plus a molecular rotational excitation $\ell=1$, i.e., the molecule is now not only translated but is also excited rotationally to the $\ell=1$ state. S_3 shows qualitatively the same features. In contrast, in S_1 the roton-maxon wings are negligibly small. The primary peak has almost all the strength of the spectrum, because the dipole field directly couples to the $J=1$ excitation energy of the molecule, the energy of which is much lower than the roton. Thus, for $J=1$ alone the absorption spectrum looks like a gas-phase spectrum and can thus be described purely in terms of an effective rotational constant B_{eff} which determines the location of the single peak.

In principle, there is an infinite series of roton-maxon wings for each ℓ , shifted by $B\ell(\ell+1)$, with decreasing strength. However, with increasing energy $\hbar\omega$, multiphonon processes presumably become important. For example, in pure helium, these processes become important for energies above approximately 25 K, above which the dynamic struc-

ture function $S(k, \omega)$ is dominated by multiphonon excitations.⁶¹ In our implementation of CBF theory, only one-phonon processes are taken into account. Two technical details of our calculations are presented in the appendixes. The first is the necessity to introduce a cutoff in the Legendre expansion of $g(r, \cos \alpha)$ (Appendix B). The second is a comparison of the effects of making the various phenomenological corrections to the self-energy discussed in Sec. II A (Appendix C).

	CBF	Experiment (Ref. 1)	ΔI (CBF)	ΔI (expt.)
HCN	0.857 ± 0.019	0.814	1.90 ± 0.29	2.61
DCN	0.863 ± 0.016	0.830	2.22 ± 0.31	2.87

ture function $S(k, \omega)$ is dominated by multiphonon excitations.⁶¹ In our implementation of CBF theory, only one-phonon processes are taken into account.

Two technical details of our calculations are presented in the appendixes. The first is the necessity to introduce a cutoff in the Legendre expansion of $g(r, \cos \alpha)$ (Appendix B). The second is a comparison of the effects of making the various phenomenological corrections to the self-energy discussed in Sec. II A (Appendix C).

C. Effective rotational constant B_{eff} of HCN and DCN in ^4He

From the position of the single peak in the absorption spectrum S_1 we can obtain the rotational excitation energy of the $J=1$ excitation, $\hbar\omega_1$, from which we can obtain an effective rotational constant of B_{eff} assuming a free rotor spectrum:

$$\hbar\omega_1 = 2B_{\text{eff}}.$$

This is the direct analog of the procedure used to obtain an experimental measurement of B_{eff} in Refs. 1 and 2. Table II compares the effective rotational constant of HCN and DCN, obtained from $J=1$ only in this manner, with the corresponding measured values of Ref. 1. The statistical error of B_{eff} shown in the table is propagated from the DMC ground-state calculation of $g(r, \cos \alpha)$. The values of B_{eff} are in overall good agreement with the experimental values, agreeing to within 5% for both molecules, although the error bars ($\sim 2\%$) are unfortunately too large to confirm the experimental determination of a slightly smaller ($\sim 1.5\%$) ratio B_{eff}/B for the lighter HCN than for DCN. For both HCN and DCN, the calculated values of B_{eff} are slightly larger than the experimental values. Such behavior of CBF theory to produce somewhat higher excitation energies than the corresponding experimental (exact) values has been observed in other cases.³² One remedy for this is to apply phenomenological corrections to all terms in the energy denominator of $\Sigma_J(\omega)$ as we have explained in Sec. II A. The values given in Table II were obtained by making such a correction only to the Bijl-Feynman spectrum for bulk helium, i.e., replacing this by the experimental collective excitation spectrum, but not modifying $B\ell(\ell+1)$. The additional effect of this further correction is summarized in Table III where we see a slight improvement of B_{eff} in its agreement with the experi-

TABLE III. Comparison of the calculated ratio B_{eff}/B_0 for HCN obtained with and without the phenomenological corrections explained in the text. The four entries correspond to the four possible combinations of corrections in the energy denominator of the self-energy $\Sigma_J(\omega)$: (i) the Bijl-Feynman spectrum (left column) or the experimental spectrum (right column), and (ii) the gas-phase rotational energies (top row) or self-consistent solution of the rotational energies in helium, Eqs. (C1) and (C2) (bottom row).

	Bijl-Feynman	Expt. bulk spectrum
$B\ell(\ell+1)$	0.913	0.857
$\hbar\omega_\ell$	0.910	0.841

mental values upon making a self-consistent replacement of $B\ell(\ell+1)$ by $\hbar\omega_\ell$. Table III shows that the biggest improvement derives from the replacement of the Bijl-Feynman spectrum by the experimental bulk spectrum. Further improvement could presumably be achieved by replacing the bare molecular mass M by the effective mass M_{eff} of HCN and DCN moving in ^4He , if these quantities were known. However, we have checked that realistic changes in these quantities would not change the qualitative behavior of any of our results. These checks and relevant details for implementation of the phenomenological corrections are provided in Appendix C.

Given that the value of B_{eff} obtained here for HCN in bulk ^4He is in good agreement with that measured in large droplets ($N > 1000$ helium atoms), it is interesting to compare also with the corresponding values calculated for small clusters¹⁴ (no experimental measurements have been made yet on small clusters). As noted in Sec. I, calculations of the $J=1$ excitation by the POITSE methodology show that the resulting fitted value B_{eff} does not converge to the large droplet value by $N=25$, in contrast to the behavior of the heavier molecules such as OCS and SF_6 . For these molecules, B_{eff} converges to the corresponding droplet value before the first solvation shell is complete.^{4,17,18,20,62,63} There are several possible reasons for this difference. First, our analysis for HCN in bulk ^4He shows that a light rotating molecule leads to generation of collective excitations that are extended in space (phonons and rotons) instead of to formation of a local nonsuperfluid density in the first solvation shell that can adiabatically follow the molecular rotation.⁴ The cluster size dependence for these two different mechanisms might reasonably be expected to be very different, with the coupling to extended modes requiring more than a single solvation shell to approach its bulk character. A second possible explanation is that the projection operator \hat{A} used in Ref. 14 accesses a higher $J=1$ state than the state associated with the rotation of the molecule, thereby causing the targeted excitation to overshoot not only the large droplet value but also the gas-phase rotational energy. This effect was already seen in the POITSE excitation spectra of the smallest clusters calculated in Ref. 14, where multiple peaks were found, one of which was consistently above the gas-phase rotational energy. For $N=1$, comparison with the corresponding result obtained by the collocation method³⁵ confirmed that this excitation is indeed a higher-lying $J=1$ level. The POITSE method relies

on having a good projection operator $\hat{A}\Psi_0$ which has sufficient overlap with the desired excited state. In this case one seeks a rotation of the molecule, but one that nevertheless involves considerable correlation of the molecule with the helium, as is evident from the second term in the CBF excitation operator, Eq. (2.7). In contrast, the projector that has been used in both POITSE (Refs. 14 and 17) and related methods¹⁸ to date is a free molecular rotor function, which corresponds only to the first term in Eq. (2.7). This suggests that it will be worthwhile to use the full stationary CBF excitation operator $\hat{A} = \delta U$ in a POITSE calculation, as we have already proposed in Sec. II C above.

The situation seems to be opposite for heavier rotors in ^4He , namely, here the direct approaches by evaluation and inversion of imaginary time correlation functions can provide a better description of the rotational dynamics. Thus, POITSE and related approaches are able to obtain accurate values for B_{eff} for OCS,^{17,18} but our current implementation of CBF is not expected to be reliable in this case, as we have noted in Sec. II A. We expect that working in the frame of the molecule would improve the CBF description to account also for the adiabatic following of ^4He around such heavy rotors.

D. Effective distortion constant D_{eff} of HCN and DCN in ^4He

We can use sharp spectral peaks for higher J values and fit to the spectroscopic energy levels for a nonrigid linear rotor, $B_J(J+1) - D(J(J+1))^2$,⁶⁴ where D is the centrifugal distortion constant. However, this fit should be used with considerable caution, for two reasons. First, as we have seen in Sec. IV B, the deviations of the $J=0 \rightarrow 2$ and $0 \rightarrow 3$ transitions from an effective linear rotor are very large and have nothing to do with a true centrifugal distortion that might arise from a coupling of the molecular rotation to either a molecular or a localized helium vibration. In particular, these higher transitions are split into two peaks which cannot both be fit by a simple phenomenological centrifugal distortion term. Second, both the statistical errors from the DMC and the errors stemming from the approximations used in CBF (see Sec. II above) grow with J , leading to larger overall errors associated with the peaks for higher J values. Nevertheless, by direct analogy again with the experimental procedure of fitting to spectral line positions, we can make a phenomenological fit to the $J=1$ spectral line together with the lowest spectral peak for each of the $J=2$ and $J=3$ spectra. The result is that because of the downward shift of the $J=2$ and $J=3$ lines induced by coupling to the roton-maxon excitations, we find a very large value of the fitted effective centrifugal distortion constant D_{eff} . Thus, e.g., for HCN, while we obtain a value $B_{\text{eff}} = \omega_1/2 = 1.266 \text{ cm}^{-1}$ (1.822 K) from the $J=1$ line only, fitting the $J=1$ and first $J=2$ peaks yields $B_{\text{eff}} = 1.346 \text{ cm}^{-1}$ (1.937 K) and $D_{\text{eff}} = 0.040 \text{ cm}^{-1}$ (0.058 K), and further fitting the $J=1$ and first $J=2$ and $J=3$ peaks all together yields $B_{\text{eff}} = 1.320 \text{ cm}^{-1}$ (1.899 K) and $D_{\text{eff}} = 0.035 \text{ cm}^{-1}$ (0.050 K). These values of D_{eff} are vastly enhanced over the gas-phase value of the centrifugal distortion constant for HCN, $D = 2.9 \times 10^{-6} \text{ cm}^{-1}$,⁶⁵ showing an increase of four orders of magnitude. Similar enhancements of several orders of magnitude have been observed in

TABLE IV. The effective distortion constant D_{eff} and the ratios D_{eff}/B and $D_{\text{eff}}/B_{\text{eff}}$ calculated for HCN in helium by the present combination of CBF and DMC, compared to the corresponding ratios derived from experimental measurements for OCS in helium droplets (Ref. 66). We also show the corresponding values calculated for HCN within the pseudohydrodynamic model of Sec. IV F. The last two columns give the gas-phase reference values of the spectroscopic constants B and D for the two molecules.

	D_{eff} (cm^{-1})	D_{eff}/B	$D_{\text{eff}}/B_{\text{eff}}$	B (cm^{-1})	D (cm^{-1})
HCN	0.035	0.0237	0.0265	1.478 (Ref. 65)	2.9×10^{-6} (Ref. 65)
OCS(expt.) (Ref. 66)	0.0004	0.00197	0.00546	0.0732	0.438×10^{-7}
HCN(pseudohydro.)	0.00568	0.00384	0.00412		

experimental fitted values of D_{eff} to multiple spectral lines for heavier molecules³ and no theoretical explanation for these large enhancements has been given.

The fitting constant D_{eff} for HCN in helium and the gas-phase centrifugal distortion constant D measure different physical effects. D is the usual measure of distortion of the linear rotor spectrum due to the nonrigid nature of HCN, which results in centrifugal forces acting on the component atoms as the molecule rotates, and hence in increased moments of inertia and lower rotational energy levels. D_{eff} is a measure of the deviation from the effective linear rotor spectrum caused instead, in the case of the weakly anisotropic HCN molecule, by the ‘‘back-flow’’ of the surrounding helium. As our CBF results clearly show, the ‘‘back flow’’ effect on the energy spectrum is much bigger than centrifugal distortion of the bare molecule. Thus the observed enhancement factor with respect to the gas-phase value, D_{eff}/D , is not significant, and D can be neglected in the discussion of rotational spectra of molecules in helium.

In the first column of Table IV we compare the effective distortion constant D_{eff} of HCN (from fitting to our CBF results) and OCS (fitted to experimental data) in helium. We also show values of D_{eff} obtained for HCN in a pseudohydrodynamic limit model, discussed in Sec. IV F. In the second and third columns, we show the respective ratios D_{eff}/B and $D_{\text{eff}}/B_{\text{eff}}$, i.e., we normalize D_{eff} such that all (free) linear rotor spectra would collapse on the same curve $J(J+1)$.

We see from Table IV that regardless of whether we use either D_{eff} , or D_{eff}/B , or $D_{\text{eff}}/B_{\text{eff}}$ as a measure of distortion of the linear rotor spectrum, the HCN spectrum of excitation energies deviates considerably more from the linear rotor spectrum than does the spectrum of the heavier OCS molecule. We also see that the ratio $D_{\text{eff}}/B_{\text{eff}}$ is similar for OCS and HCN in the pseudohydrodynamic model. A possible explanation for this last observation is given in Sec. IV F below.

The large value of D_{eff} for HCN calculated here is a direct consequence of the high density of states in bulk helium near the roton minimum and maxon maximum, which are missing in the hydrodynamic limit model. This high density of states gives rise to a downward shift of the lower component of the split peaks for higher J states, as discussed in Sec. IV B above and explained in detail in Appendix A. It also explains the greater distortion of the linear rotor spectrum compared to the distortion measured for OCS, since the considerably lower energy rotational excited states of OCS do not couple

as effectively to the roton and maxon states as the rotational states of the lighter HCN molecule.

E. Rotation lifetimes and homogeneous linewidth

The self-energy Σ_J has a small, but finite imaginary part, which leads to a finite life-time $\tau = 1/\text{Im}\Sigma_J$ of the rotational excitation, i.e., to homogeneous line broadening of the rotational absorption spectra. $\text{Im}\Sigma_J$ results from the principal value integration $\int dp$ in Eq. (2.34) that is made when the energy denominator vanishes at some momentum $p = p_0$,

$$\text{Im}\Sigma_J = \frac{2B^2\rho}{2J+1} \sum_{\ell'} \frac{p_0^2}{S(p_0)} \frac{\sum_{\ell} \tilde{L}(J, \ell', \ell) g_{\ell'}^2(p_0)}{d\epsilon(p_0)/dp + \hbar^2 p_0/M} \quad (4.2)$$

with p_0 defined by

$$B\ell(\ell+1) + \epsilon(p_0) + \frac{\hbar^2 p_0^2}{2M} = \hbar\omega. \quad (4.3)$$

The lifetime is obtained by summing the contribution from all poles p_0 . For calculation of the $J=1$ excitation, Eq. (4.3) only has a solution for $\ell=0$ and hence there is only one pole, because $\hbar\omega < B\ell(\ell+1)$. From the selection rules (2.35), we find that $\ell'=1$ and hence we obtain the estimate of linewidth

$$\text{Im}\Sigma_{J=1} = \frac{2}{3} B^2 \rho \frac{p_0^2}{S(p_0)} \frac{\tilde{L}(1,1,0) g_1^2(p_0)}{d\epsilon(p_0)/dp + \hbar^2 p_0/M}. \quad (4.4)$$

Unfortunately the value of the momentum at the poles for HCN and DCN is very small: $p_0 = 0.19 \text{ \AA}^{-1}$ for HCN and $p_0 = 0.15 \text{ \AA}^{-1}$ for DCN. These momentum values are too small for the corresponding Legendre component of the pair-correlation function $g_1(p_0)$ to be a reliable estimate. This can be seen by considering for simplicity the Fourier transform of a periodic function with period s . The corresponding wave number p is discrete with smallest nonzero wave number equal to $p_{\text{min}} = 2\pi/s$. In our case, $s = 23.0 \text{ \AA}$ is the simulation box length. This results in a minimum wave number $p_{\text{min}} = 0.27 \text{ \AA}^{-1}$, which is larger than the desired pole momentum values p_0 for HCN and DCN given above. Furthermore, we have the limiting behavior $g_1(p) \sim p$ for $p \rightarrow 0$. Hence the Legendre component at the pole $g_1(p_0)$ is small, resulting also in a small value of $\text{Im}\Sigma_{J=1}$. This explains the small width of the $J=1$ line evident in Figs. 4 and 5. How-

ever, since the statistical error of $g_1(p)$ for small p is of the order of $g_1(p)$ itself, we are not able to extract a reliable quantitative estimate of the $J=1$ lifetime and the associated linewidth.

F. Hydrodynamic limit

Hydrodynamical models have been used to describe rotations of heavy molecules with large moments of inertia solvated in ^4He .^{4,7,20} As we have noted already in the Introduction, these models fail for light rotors like HCN when based on assumptions of adiabatic following. In this section we show that independently of any assumption of adiabatic following, any analysis of light rotor rotation involving hydrodynamic coupling to long-wavelength helium modes cannot provide an adequate description of the coupled molecule-helium excitations dynamics because of the absence of coupling of rotational levels to ^4He excitations of higher energy than the long-wavelength phonon modes, i.e., to rotons and maxons.

We can simulate a hydrodynamic description of the ^4He environment by replacing p -dependent ^4He quantities by their low- p expansion:

$$S(p) \rightarrow \frac{\hbar p}{2mc}, \quad (4.5)$$

$$\varepsilon(p) \rightarrow \hbar c p. \quad (4.6)$$

For simplicity, we keep the molecule- ^4He pair distribution $g(r, \cos \alpha)$ we have obtained from the quantum-mechanical DMC calculation. Therefore, our toy model is not a true hydrodynamical model, which would require calculation of $g(r, \cos \alpha)$ for HCN solvated in a hydrodynamic environment. It should be noted that this “pseudohydrodynamic” model does not assume adiabatic following of the ^4He .^{4,11} In the present context, “hydrodynamic” refers simply to the coupling to bulk helium modes with long wavelength.

In Fig. 6 we show the absorption spectra S_J , $J=1,2,3$ for HCN that are obtained with this pseudohydrodynamic model. These spectra show only sharp peaks and no broad bands, as expected from the discussion in Sec. IV B that assigned the broad bands to coupling to collective excitations in the maxon-roton region. Also, only a single spectral line is found for all three J levels. According to the analysis in Sec. IV B and in Appendix A (see also Fig. 7), this is also consistent with the lack of coupling to maxon-roton states. Fitting the positions of the three spectral peaks results in a good fit to a linear rotor spectrum, yielding effective spectroscopic constants $B_{\text{eff}}=1.376 \text{ cm}^{-1}$ (1.980 K) and $D_{\text{eff}}=0.00568 \text{ cm}^{-1}$ (0.00817 K), respectively, and a corresponding ratio value $B_{\text{eff}}/B_0=0.931$. The reduction in rotational constant is significantly less than the experimentally observed reduction of 0.815, amounting to only $\sim 36\%$ of the experimental reduction. This large discrepancy with the observed change of the rotational constant, in contrast to the good agreement achieved in Sec. IV C from coupling to the true helium excitation spectrum further confirms that the

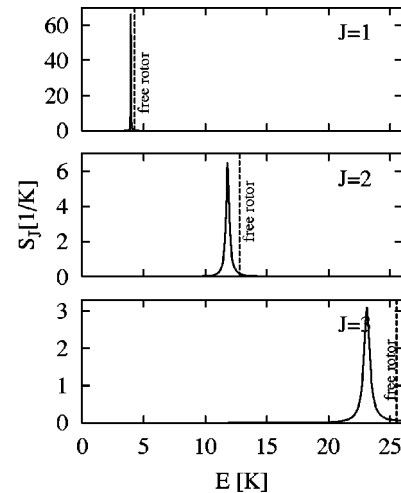


FIG. 6. The absorption spectra $S_J(\omega)$, $J=1,2,3$, for HCN obtained with the “pseudohydrodynamic model” in which the bulk ^4He is replaced by a hydrodynamic model fluid having only long-wavelength (phonon) modes, i.e., possessing linear dispersion. The simulation is made with $N=256$ ^4He in a box subject to periodic boundary condition and a length of 23.0 Å. The dashed lines indicate the corresponding spectral positions for HCN in the gas phase (Ref. 65).

maxon-roton regime of excitations has a strong influence on the rotation of light rotors in ^4He . It is therefore essential for a reliable model to either directly (as in the present CBF approach) or indirectly (e.g., as in the POITSE approach) allow for coupling of the rotational levels with those excitations.

The effective distortion constant D_{eff} is significantly reduced with respect to the full CBF result (see Table IV), while its ratio $D_{\text{eff}}/B_{\text{eff}}$ is similar to the corresponding ratio for OCS. This suggests that the effective distortion constant of OCS may be rationalized as resulting from coupling to long-wavelength phonons. Within the present CBF analysis, this is consistent with the observation that for OCS with a gas phase rotation constant $B=0.2029 \text{ cm}^{-1}$ (0.2920 K), the roton excitations are too high in energy to couple effectively to the molecular rotation. However, for OCS the local coupling to helium⁴ needs also to be taken into account for a full analysis, as discussed in Sec. II A above. Consequently a consistent analysis of both B_{eff} and D_{eff} for OCS will most likely benefit from reformulating the CBF theory in the molecular frame, as suggested in Sec. II A.

Finally, it is interesting to note that this pseudohydrodynamic model severely *underestimates* the change of the rotational constant for HCN, as opposed to the overestimation for HCN that was obtained from the previous hydrodynamic model of Ref. 7 that assumed complete adiabatic following of the molecular rotation by helium.

V. CONCLUSIONS

In this paper, we have derived the dynamic equations for molecular rotations in bulk ^4He within the formalism of CBF theory and applied them to HCN and DCN in superfluid bulk ^4He at $T=0$. For that purpose we have combined DMC

calculations for the required ground-state properties with the CBF theory for excitations. Energy levels, absorption spectra, and spectroscopic constants for rotational excitations of the HCN and DCN molecules were calculated from this combined theoretical approach which allows for coupling to collective ^4He excitations. Our results for the effective rotational constants of HCN and DCN are seen to be in good agreement with the corresponding experimentally determined values.¹ The CBF values are slightly higher than the experimental results (by $\sim 5\%$ of B , corresponding to $\sim 25\%$ of the reduction $B - B_{\text{eff}}$), with about half of the difference being contained within the statistical error. We saw that the CBF values could be improved with systematic incorporation of more phenomenological input to the self-energy. The statistical error derives from the DMC calculation of the molecule-helium pair distribution function and is hard to reduce further without imposing excessive computational requirements (the required sampling grows as the inverse square of the statistical error). For the present calculations with HCN and DCN, the statistical error of DMC is unfortunately too large to determine whether the experimentally observed small isotope effect ($\sim 1.5\%$) is correctly predicted by CBF.

An attractive feature of the CBF approach is the ability to calculate the full microwave absorption spectra at zero temperature. We calculated the spectra of the dipole, quadrupole, and octopole transitions of HCN, corresponding to $J=0 \rightarrow 1$, $0 \rightarrow 2$, and $0 \rightarrow 3$. The $J=0 \rightarrow 1$ transition is found to be very sharp and the dipole spectrum to have almost no features apart from the single Lorentzian peak centered at the $J=1$ excitation energy. In contrast, the $J=0 \rightarrow 2$ and $J=0 \rightarrow 3$ transitions show weak phonon-maxon-rotor bands as well as secondary peaks. Both of these features are caused by the strong coupling of the molecule rotation to the roton and maxon excitations of ^4He . This strong coupling is also responsible for the large values of the effective distortion constant D_{eff} that result from fitting the primary peaks of the rotational excitation spectrum to the effective nonrigid linear rotor energy level expression $BJ(J+1) - D[J(J+1)]^2$. The importance of the phonon-maxon-rotor spectrum was further highlighted by a comparative calculation where the rotational excitations are calculated with coupling to a phonon dispersion mode alone (Sec. IV F). In this pseudohydrodynamical model that lacks roton and maxon excitations, a much simpler absorption spectrum S_J was found that possesses only a single peak for all J values and no broad sidebands. The resulting empirically fit rotation constant is considerably higher than the experimental values, and smaller values of the effective distortion constant are seen. This shows that the coupling to the roton and maxon excitations of helium increases the deviation from the linear rotor spectrum. This coupling is strong for HCN and other light molecules, due to the vicinity of the $J=2$ and $J=3$ rotational levels to the roton energy.

A key feature of our CBF results is their demonstration that the coupling to phonons and rotons of the bulk helium environment accounts quantitatively for the observed reduction of the effective rotational constant B_{eff} for HCN and DCN. For these light molecules, coupling to localized

modes, e.g., as manifested by adiabatic following of some fraction of the first solvation shell helium density,⁴ can therefore be at most a very minor effect in the reduction of B_{eff} .

As far as the methodology is concerned, the combination of DMC and CBF employed here facilitates the calculation of excitation energies in the CBF approximation because of the ease of implementing DMC, which provides the ground-state pair distribution $g(r, \cos \alpha)$ needed for a CBF calculation. On the other hand, DMC is computationally much more expensive than the alternative of a full CBF calculation of both ground state and excitations. Even after extensive sampling, the statistical error of the ^4He -HCN and ^4He -DCN pair distribution function $g(r, \cos \alpha)$ was too large to be able to detect a statistically reliable difference between the rotational constants of the two isotopic species. Furthermore, with currently feasible simulation box sizes containing $N = 256$ ^4He atoms, we cannot reliably account for the long-range (small wavelength) correlations which are needed for the calculation of the homogeneous linewidth (Sec. IV E). Ground-state CBF, in contrast, is particularly reliable for long-range properties, while it yields only approximations to short-range properties, like the peak density of the first shell of ^4He around the correlation hole of a ^4He atom or a molecule. Thus, neither of these two approaches alone provides all the required ingredients to accurately obtain both the very small isotopic dependences of rotational constants and linewidths for the HCN and DCN isotopomers.

In this work, we have considered the simplest implementation of the CBF analysis for molecular excitations in ^4He , by assuming an infinite bulk ^4He matrix. However, matrix isolation spectroscopy experiments are performed in droplets consisting of a few thousands of ^4He atoms. As noted above, the inhomogeneous environment has been shown¹³ to possibly cause inhomogeneous line broadening and may be responsible for the M -splitting of the observed $R(0)$ line for HCN.² Another simplification made in the current CBF analysis was the disregard of coupling of rotation and translations of the molecule. This is justified at $T=0$. At finite temperatures however, translational excitations will be populated, and these provide another source for inhomogeneous line broadening. The present CBF calculations can be generalized to molecules embedded in a finite quantum cluster which would allow quantification of the effect of a long-range inhomogeneous helium environment (as distinct from the inhomogeneity in the local solvation shell around the molecule which is incorporated in this work) on the rotational dynamics of molecules. Finally we note that extension of the CBF approach presented here to heavy rotors like OCS and SF_6 may be feasible if the minimization of the action integral, Eq. (2.8), is performed in a frame rotating with the molecule, thus allowing also for coupling to ^4He excitations localized around the molecule and for adiabatic following of some local ^4He density.

ACKNOWLEDGMENTS

This work was supported by the Miller Institute for Basic Research in Science and by the NSF under Grant No. CHE-010754. The authors would like to thank the Central Infor-

mation Services of the Kepler University, Linz, Austria for providing computational resources.

APPENDIX A: SELF-CONSISTENT SOLUTION OF Eq. (2.33)

The absorption spectra $S_J(\omega)$ of Eqs. (2.38) and (2.36) are complete descriptions of the spectrum in that they contain all the information about excitation energies that CBF theory can provide. However, it is instructive to take a closer look at precisely how the sharp peaks in $S_J(\omega)$ arise from Eqs. (2.38) and (2.36). The present discussion follows closely the discussion of appendix A in Ref. 26.

With the abbreviation

$$\gamma_J(\omega) = BJ(J+1) + \text{Re}\Sigma_J(\omega)$$

we can write the spectrum as

$$S_J(\omega) = \frac{\text{Im}\Sigma_J(\omega)}{[\gamma_J(\omega) - \hbar\omega]^2 + [\text{Im}\Sigma_J(\omega)]^2}.$$

Hence sharp peaks, i.e., long lifetimes of excitations⁶⁷ of energy $\hbar\omega_0$, occur when $\gamma_J(\omega_0) = \hbar\omega_0$ and $\text{Im}\Sigma_J(\omega)$ is small. In this situation, $S_J(\omega)$ is small everywhere except near $\omega = \omega_0$. In the vicinity of this region we can expand

$$\begin{aligned} \gamma_J(\omega) - \hbar\omega &= \alpha_J \hbar(\omega - \omega_0) \\ \text{with } \alpha_J &= \left[\frac{d\text{Re}\Sigma_J(\omega)}{d\hbar\omega} - 1 \right]_{\omega=\omega_0}, \end{aligned}$$

and obtain a Lorentzian centered at ω_0 ,

$$S_J(\omega) = \frac{\epsilon_J}{\hbar^2 \alpha_J^2 (\omega - \omega_0)^2 + \epsilon_J^2}.$$

Here we have assumed that $\text{Im}\Sigma_J(\omega)$ varies very little in the region close to ω_0 and can consequently be replaced by $\epsilon_J = \text{Im}\Sigma_J(\omega_0)$. The weight of the peak is obtained by integration of the peak

$$\int d\hbar\omega S_J(\omega) = \frac{\pi}{|\alpha_J|}.$$

Hence we find the position of a peak by solving the equation

$$\gamma_J(\omega) - \hbar\omega = 0$$

for one or several roots ω_i . We obtain the width of the peak from $\text{Im}\Sigma_J(\omega_i)$ and its weight from $|d\gamma_J(\omega_i)/d\omega - 1|^{-1}$. All this applies only when $\text{Im}\Sigma_J(\omega_i)$ is small.

In Fig. 7 we show $\gamma_J(\omega) - \hbar\omega$ as a function of $\hbar\omega$ for $J=2$. In the range shown in the plots, $\gamma_J(\omega) - \hbar\omega$ has two roots, $\omega^{(1)}$ and $\omega^{(2)}$, indicated by black points. Since the imaginary parts of $\Sigma_J(\omega^{(1)})$ is small, $S_J(\omega)$ has a sharp peak at $\omega^{(1)}$, see Fig. 5. In contrast, $\text{Im}\Sigma_J(\omega^{(2)})$ is much larger, resulting in a broad peak at $\omega^{(2)}$. Furthermore, both the real

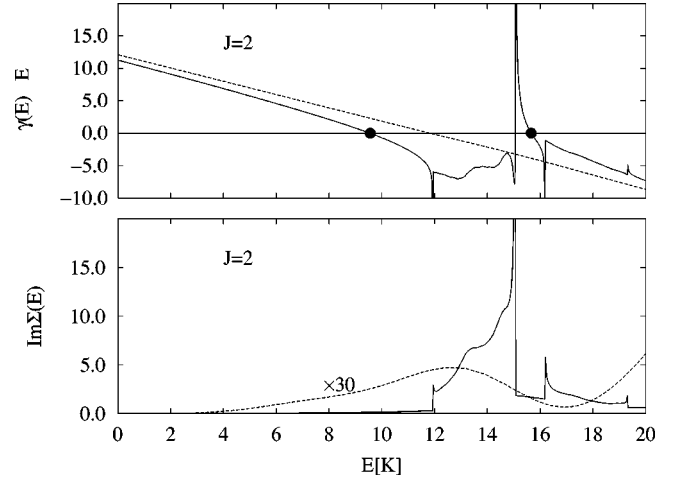


FIG. 7. Illustration of procedure for obtaining excitation energies from Eq. (2.33). The upper panel shows $\gamma_J(\omega) - \hbar\omega$ for $J=2$, where $\gamma_J(\omega) \equiv BJ(J+1) + \text{Re}\Sigma_J(\omega)$. The points emphasize the zeros of $\gamma_J(\omega) - \hbar\omega$, which are the excitation energies for $J=2$. For comparison, the dashed line shows $\gamma_J(\omega) - \hbar\omega$, $J=2$, from our pseudohydrodynamic model, see Sec. IV F, where $\gamma_J(\omega) = \hbar\omega$ has only one solution, leading to the single peak shown in Fig. 6. The lower panel shows $\text{Im}\Sigma_J(\omega)$ for $J=2$. Again, the dashed line indicates the corresponding result of the pseudohydrodynamic model. See text for a full discussion.

and imaginary parts of $\Sigma_J(\omega)$ vary significantly near $\omega^{(2)}$, so that the peak is no longer Lorentzian. A broad band can be seen between the two peaks in Fig. 5. This broad band stems from the large values for $\text{Im}\Sigma_J(\omega)$ when $\hbar\omega$ lies in the roton-maxon band of the density of states, which is large between the two extremas of $\epsilon(p) + \hbar^2 p^2 / 2M$ (see lowest panel of Fig. 5). It is easy to show that the density of states, as well as $\text{Im}\Sigma_J(\omega)$, diverges as the inverse square root of the energy at the extremas of $\epsilon(p) + \hbar^2 p^2 / 2M$ (see lower panel of Fig. 7). The real component $\text{Re}\Sigma_J(\omega)$ also diverges as the inverse square root, but it does so on the “outer” sides of roton-maxon band (see upper panel of Fig. 7). These two divergences of $\text{Re}\Sigma_J(\omega)$ and hence of $\gamma_J(\omega) - \hbar\omega$ at the roton-maxon band are clearly responsible for the occurrence of two roots $\omega^{(1)}$ and $\omega^{(2)}$. In the pseudohydrodynamical model presented in Sec. IV F we retain only the linear phonon dispersion and there is no roton-maxon band. Consequently, $\text{Re}\Sigma_J(\omega)$ does not diverge anywhere and we find only a single peak for each J in the pseudohydrodynamic calculations.

APPENDIX B: ℓ CUTOFF FOR $g_\ell(p)$

Since $g(r, \cos \alpha)$, and therefore $g_\ell(p)$, is affected by statistical noise, the self-energy $\Sigma_J(\omega)$ is also affected by this. For large ℓ , $g_\ell(p)$ is small and the noise will exceed the true value of $g_\ell(p)$. But $\Sigma_J(\omega)$ is a functional of $g_\ell^2(p)$, i.e., for large ℓ , the summation over ℓ in Eq. (2.34) adds only noise to Σ_J instead of converging. For that reason we introduce a cutoff ℓ_{cut} to $g_\ell(p)$, such that $g_\ell(p) = 0$ for $\ell > \ell_{\text{cut}}$. In Fig. 8, we show the ratio B_{eff}/B_0 for HCN as a function of the cutoff ℓ_{cut} , where the phenomenological self-energy with the

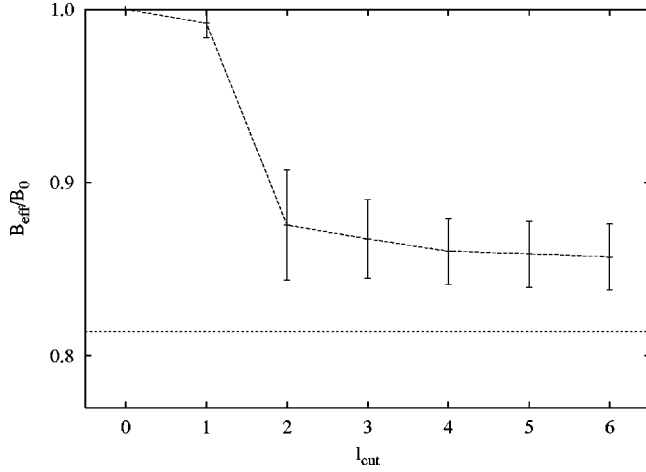


FIG. 8. The effective rotational constant ratio B_{eff}/B_0 as a function of the cutoff l_{cut} for HCN in bulk ^4He , approximated by $N = 256$ ^4He in a box subject to periodic boundary conditions. We have truncated the Legendre expansion of the pair distribution $g(r, \alpha)$ at l_{cut} . The expansion has reached convergence at a value slightly higher than the experimentally measured ratio (Ref. 1) which is indicated by the horizontal line.

experimental rather than the Bijl-Feynman excitation spectrum was used in the denominator. Figure 8 shows clearly that for HCN the largest contribution to $\Sigma_J(\omega)$ comes from $\ell = 2$, i.e., the quadrupole deviation from a spherical distribution around the molecule. Beyond $\ell > 4$, $g_\ell(p)$ contributes very little to Σ_J , therefore we choose $l_{\text{cut}} = 6$. The uncertainty associated with l_{cut} is much smaller than the statistical error of B_{eff}/B_0 that is propagated from the error of $g(r, \cos \alpha)$.

APPENDIX C: CORRECTION TO $\Sigma_J(\omega)$

The self-energy $\Sigma_J(\omega)$ (2.34) was obtained by allowing for fluctuations of two-body correlations and using the uniform limit approximation. As mentioned above, we can try to improve $\Sigma_J(\omega)$ without changing its analytic form, but instead by introducing a phenomenological energy denominator, obtained by (i) using the experimental excitation spectrum^{15,54} instead of the Bijl-Feynman spectrum, (ii) using the effective mass of HCN or DCN instead of the bare mass in $\hbar^2 p^2/2M$, or (iii) using $\hbar\omega_\ell$ instead of $B\ell(\ell+1)$, as well as by combinations of these corrections.

For the last replacement, we have to solve Eq. (2.33) self-consistently not only for $J=1$, but simultaneously for all J , because of the occurrence of $\hbar\omega_\ell$ in Σ_J . Hence we solve the set of equations

$$\hbar\omega_J = BJ(J+1) + \text{Re}\Sigma_J(\omega_J), \quad J = 1, \dots, J_{\text{max}} \quad (\text{C1})$$

with

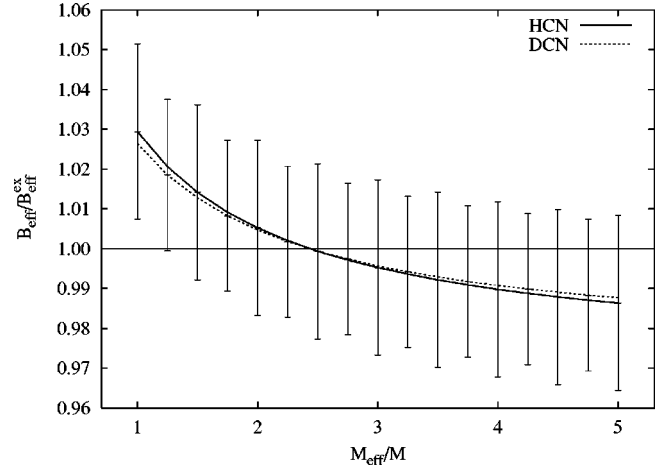


FIG. 9. The error of calculated vs experimental effective rotational constant, $B_{\text{eff}}/B_{\text{eff}}^{\text{ex}}$, for HCN and DCN as a function of the effective mass ratio M_{eff}/M . That the intersections of the curves with $B_{\text{eff}}/B_{\text{eff}}^{\text{ex}} = 1$ occurs at the same values of M_{eff}/M is clearly not statistically significant because of the large error bars. The value of $B_{\text{eff}}^{\text{ex}}$ is taken from Ref. 1. See Appendix C for a discussion of the phenomenological corrections used in this figure.

$$\begin{aligned} \Sigma_J(\omega_J) = & -B^2 \frac{(4\pi)^2 \rho}{2J+1} \sum_{\ell} \int \frac{dp}{(2\pi)^3} \frac{p^2}{S(p)} \\ & \sum_{\ell'} \tilde{L}(J, \ell', \ell) g_{\ell'}^2(p) \\ & \times \frac{1}{\hbar\omega_\ell + \epsilon(p) + \hbar^2 p^2/2M - \hbar\omega_J}. \quad (\text{C2}) \end{aligned}$$

We take the real part of the self-energy, assuming that the imaginary part is small, since only then we have well-defined excitations, albeit decaying ones. We note that for $J > 1$, each one of Eqs. (C1) has more than one solution, but we restrict ourselves to the solution which we believe corresponds to the effective rotational excitation of the molecule, i.e., to the primary peak of S_J . This correspondence can only be established up to $J=3$, hence we have to restrict ourselves to $J_{\text{max}}=3$. For $J > 3$ we use $BJ(J+1)$. In our view, solving Eqs. (C1) for all other solutions as well and retaining the imaginary part of $\Sigma_J(\omega)$ would stretch the validity of a phenomenological correction of $\Sigma_J(\omega)$ and is therefore not warranted.

The resulting four combinations of corrections (i) and (iii) for $\Sigma_J(\omega)$ for HCN in bulk ^4He are compared in Table III. Clearly, the replacement of the Bijl-Feynman spectrum by the experimental excitation spectrum constitutes a significant correction of $\Sigma_J(\omega)$ and manages to come close to the experimental values of B_{eff} . On the other hand, the self-consistent replacement of $B\ell(\ell+1)$ by $\hbar\omega_\ell$ leads only to a minor further reduction of B_{eff} , almost within the statistical error of $\Sigma_J(\omega)$. Hence, we do not apply the latter correction in our calculations.

It is instructive to consider the effect of the molecular mass more carefully. Unfortunately, the effective mass M_{eff} of HCN and DCN in ^4He is unknown. CBF permits the

calculation of effective masses but this would be beyond the scope of the paper. Therefore we used the bare mass M in the denominator of Eq. (C2) for all our calculations. In principle, we can turn the argument around and compare the solution ω_J of Eq. (C1) for $J=1$ with the value for ω_1 from the experiments of Ref. 1. However, on the level of CBF theory implemented in this paper, a precise prediction of the effective mass cannot be made, because ω_1 depends only weakly on M_{eff} . In Fig. 9 we show the ratios of calculated versus experimental effective rotational constant, $B_{\text{eff}}/B_{\text{eff}}^{\text{ex}}$, for HCN and DCN as a function of the effective mass ratio

M_{eff}/M , where $B_{\text{eff}}=2\omega_1$ has been obtained from Eqs. (C1) and (C2), using the experimental ^4He spectrum for $\epsilon(p)$. The error bars in Fig. 9 are estimated from the statistical error of B_{eff} obtained from Eqs. (2.33) and (2.34), with $M_{\text{eff}}=M$. The curves intersect $B_{\text{eff}}/B_{\text{eff}}^{\text{ex}}=1$ at the same values of M_{eff}/M . However, the error bars are very large, and for the entire range in Fig. 9, the dependence of B_{eff} on M_{eff} is not statistically significant. Note also that we have neglected the effect of coupling of translation and rotation on M_{eff} . Coupling would of course introduce directional dependence of M_{eff} in the molecular coordinate frame.

- ¹A. Conjunteau, C. Callegari, I. Reinhard, K.K. Lehmann, and G. Scoles, *J. Chem. Phys.* **113**, 4840 (2000).
- ²K. Nauta and R.E. Miller, *Phys. Rev. Lett.* **82**, 4480 (1999).
- ³S. Grebenev, J.P. Toennies, and A.F. Vilesov, *Science* **279**, 2083 (1998).
- ⁴Y. Kwon, P. Huang, M.V. Patel, D. Blume, and K.B. Whaley, *J. Chem. Phys.* **113**, 6469 (2000).
- ⁵Y. Kwon and K.B. Whaley, *Phys. Rev. Lett.* **83**, 4108 (1999).
- ⁶Y. Kwon and K.B. Whaley, *J. Chem. Phys.* **115**, 10 146 (2000).
- ⁷C. Callegari, A. Conjunteau, I. Reinhard, K.K. Lehmann, G. Scoles, and F. Dalfovo, *Phys. Rev. Lett.* **83**, 5058 (1999).
- ⁸K.K. Lehmann and C. Callegari, *J. Chem. Phys.* **117**, 1595 (2002).
- ⁹P. Huang, Y. Kwon, and K.B. Whaley, in *Quantum Fluids in Confinement*, edited by E. Krotscheck and J. Navarro, *Advances in Quantum Many-Body Theories*, Vol. 4 (World Scientific, Singapore, 2002), p. 91.
- ¹⁰P. Huang, T. Sachse, and K.B. Whaley (unpublished).
- ¹¹M.V. Patel, A. Viel, F. Paesani, P. Huang, and K.B. Whaley, *J. Chem. Phys.* **118**, 5011 (2003).
- ¹²K. Nauta and R.E. Miller, *J. Chem. Phys.* **115**, 8384 (2001).
- ¹³K.K. Lehmann, *Mol. Phys.* **97**, 645 (1999).
- ¹⁴A. Viel and K.B. Whaley, *J. Chem. Phys.* **115**, 10 186 (2001).
- ¹⁵R.J. Donnelly, J.A. Donnelly, and R.N. Hills, *J. Low Temp. Phys.* **44**, 471 (1981).
- ¹⁶V.S. Babichenko and Y. Kagan, *Phys. Rev. Lett.* **83**, 3458 (1999).
- ¹⁷F. Paesani, A. Viel, F.A. Gianturco, and K.B. Whaley, *Phys. Rev. Lett.* **90**, 073401 (2003).
- ¹⁸S. Moroni, A. Sarsa, S. Fantoni, K.E. Schmidt, and S. Baroni, *Phys. Rev. Lett.* **90**, 143401 (2003).
- ¹⁹D. Blume, M. Lewerenz, P. Niyaz, and K.B. Whaley, *Phys. Rev. E* **55**, 3664 (1997).
- ²⁰E. Lee, D. Farrelly, and K.B. Whaley, *Phys. Rev. Lett.* **83**, 3812 (1999).
- ²¹J. Dupont-Roc, M. Himbert, N. Pavloff, and J. Treiner, *J. Low Temp. Phys.* **81**, 31 (1990).
- ²²F. Dalfovo, *Z. Phys. D: At., Mol. Clusters* **29**, 61 (1994).
- ²³C.E. Campbell, in *Progress in Liquid Physics*, edited by C.A. Croxton (Wiley, New York, 1978), Chap. 6, pp. 213–308.
- ²⁴V. Apaja, J. Halinen, and M. Saarela, in *Condensed Matter Theories* (Nova Science Publishers, New York, 2000), Vol. 14.
- ²⁵E. Krotscheck and C.J. Tymczak, *Phys. Rev. B* **45**, 217 (1992).
- ²⁶B.E. Clements, H. Forbert, E. Krotscheck, H.J. Lauter, M. Saarela, and C.J. Tymczak, *Phys. Rev. B* **50**, 6958 (1994).
- ²⁷B.E. Clements, E. Krotscheck, and M. Saarela, *Phys. Rev. B* **55**, 5959 (1997).
- ²⁸E. Krotscheck and R. Zillich, *Phys. Rev. B* **58**, 5707 (1998).
- ²⁹S.A. Chin and E. Krotscheck, *Phys. Rev. Lett.* **74**, 1143 (1995).
- ³⁰S.A. Chin and E. Krotscheck, *Phys. Rev. B* **52**, 10 405 (1995).
- ³¹E. Krotscheck and R. Zillich, *J. Chem. Phys.* **115**, 10 161 (2001).
- ³²M. Saarela and E. Krotscheck, *J. Low Temp. Phys.* **90**, 415 (1993).
- ³³Y. Kwon, P. Huang, M.V. Patel, D. Blume, and K.B. Whaley, *J. Chem. Phys.* **113**, 6469 (2000).
- ³⁴K.M. Atkins and J.M. Hutson, *J. Chem. Phys.* **105**, 440 (1996).
- ³⁵S. Drucker, F.-M. Tao, and W. Klemperer, *J. Phys. Chem.* **99**, 2646 (1995).
- ³⁶A.R. Janzen and R.A. Aziz, *J. Chem. Phys.* **107**, 914 (1997).
- ³⁷E. Feenberg, *Theory of Quantum Fluids* (Academic Press, New York, 1969).
- ³⁸E. Krotscheck, *Phys. Rev. B* **33**, 3158 (1986).
- ³⁹E. Krotscheck and M. Saarela, *Phys. Rep.* **232**, 1 (1993).
- ⁴⁰E. Krotscheck, in *Microscopic Quantum Many-Body Theories and Their Applications*, edited by J. Navarro and A. Polls, *Lecture Notes in Physics*, Vol. 510 (Springer, New York, 1998), pp. 187–250.
- ⁴¹A. Polls and F. Mazzanti, in *Introduction to Modern Methods of Quantum Many-Body Theory and Their Applications*, edited by A. Fabrocini, S. Fantoni, and E. Krotscheck, *Series on Advances in Quantum Many Body Theory Vol. 7* (World Scientific, Singapore, 2002), p. 49.
- ⁴²D. Pines and P. Nozieres, *The Theory of Quantum Fluids* (Benjamin, New York, 1966), Vol. 1.
- ⁴³M. Saarela, in *Introduction to Modern Methods of Quantum Many-Body Theory and Their Applications*, edited by A. Fabrocini, S. Fantoni, and E. Krotscheck, *Series on Advances in Quantum Many Body Theory Vol. 7* (World Scientific, Singapore, 2002), p. 205.
- ⁴⁴R.P. Feynman, *Phys. Rev.* **94**, 262 (1954).
- ⁴⁵A.R. Edmonds, *Angular Momentum in Quantum Mechanics*, 2nd ed. (Princeton University Press, Princeton, NJ, 1960).
- ⁴⁶E. Krotscheck, J. Paaso, M. Saarela, K. Schörkhuber, and R. Zillich, *Phys. Rev. B* **58**, 12 282 (1998).
- ⁴⁷B.E. Clements, E. Krotscheck, and C.J. Tymczak, *Phys. Rev. B* **53**, 12 253 (1996).
- ⁴⁸B.E. Clements, H. Godfrin, E. Krotscheck, H. Lauter, P. Leiderer, V. Passioux, and C.J. Tymczak, *Phys. Rev. B* **53**, 12 242 (1996).
- ⁴⁹P. Huang and K.B. Whaley, *Phys. Rev. B* **67**, 155419 (2003).

- ⁵⁰D. Forster, *Hydrodynamics, Fluctuations, Broken Symmetry, and Correlation Functions*, Frontiers in Physics Vol. 47 (Benjamin, New York, 1975).
- ⁵¹E.C. Svensson, V.F. Sears, A.D.B. Woods, and P. Martel, *Phys. Rev. B* **21**, 3638 (1980).
- ⁵²H.N. Robkoff and R.B. Hallock, *Phys. Rev. B* **25**, 1572 (1982).
- ⁵³J. Boronat and J. Casulleras, *Phys. Rev. B* **49**, 8920 (1994).
- ⁵⁴R.A. Cowley and A.D.B. Woods, *Can. J. Phys.* **49**, 177 (1971).
- ⁵⁵D. Blume, M. Mladenović, M. Lewerenz, and K.B. Whaley, *J. Chem. Phys.* **110**, 5789 (1999).
- ⁵⁶V. Buch, *J. Chem. Phys.* **97**, 726 (1992).
- ⁵⁷A. Viel, M.V. Patel, P. Niyaz, and K.B. Whaley, *Comput. Phys. Commun.* **145**, 24 (2002).
- ⁵⁸J. Casulleras and J. Boronat, *Phys. Rev. B* **52**, 3654 (1995).
- ⁵⁹D.C. Rapaport, *Molecular Dynamics Simulation* (Cambridge University Press, Cambridge, England, 1995).
- ⁶⁰K. Higgins and W.H. Klemperer, *J. Chem. Phys.* **110**, 1383 (1999).
- ⁶¹A. Griffin, *Excitations in a Bose-Condensed Liquid* (Cambridge University Press, Cambridge, England, 1993).
- ⁶²J. Tang, Y. Xu, A.R.W. McKellar, and W. Jäger, *Science* **297**, 2030 (2002).
- ⁶³X.J. Xu, W. Jager, J. Tang, and A.R.W. McKellar, *Phys. Rev. Lett.* **91**, 163401 (2003).
- ⁶⁴H.W. Kroto, *Molecular Rotations* (Dover, New York, 1992).
- ⁶⁵A.G. Maki, W.B. Olson, and R.L. Sams, *J. Mol. Spectrosc.* **36**, 433 (1970).
- ⁶⁶S. Grebenev, M. Hartmann, M. Havenith, B. Sartakov, J.P. Toennies, and A.F. Vilesov, *J. Chem. Phys.* **112**, 4485 (2000).
- ⁶⁷Excitation energies of a Hermitian Hamiltonian are real. But we have eliminated the two-body correlation fluctuations $\delta u_2(\mathbf{r}_0, \mathbf{r}_1, \Omega)$ from the equations of motion (2.15) and (2.17), and the resulting equation for $\delta u_1(\mathbf{r}_0, \Omega)$ cannot be Hermitian anymore.